

Summer 2018

# Visible Light Generation of High-Valent Corrole-Manganese(V)-Oxo Intermediates and Biomimetic Studies of the Oxidation of Organic Sulfides Catalyzed by Manganese Corroles with Iodobenzene Diacetate

Davis Ray Ranburger

Western Kentucky University, d.ranburger101@gmail.com

Follow this and additional works at: <https://digitalcommons.wku.edu/theses>

 Part of the [Medicinal-Pharmaceutical Chemistry Commons](#), and the [Organic Chemistry Commons](#)

## Recommended Citation

Ranburger, Davis Ray, "Visible Light Generation of High-Valent Corrole-Manganese(V)-Oxo Intermediates and Biomimetic Studies of the Oxidation of Organic Sulfides Catalyzed by Manganese Corroles with Iodobenzene Diacetate" (2018). *Masters Theses & Specialist Projects*. Paper 3053.

<https://digitalcommons.wku.edu/theses/3053>

This Thesis is brought to you for free and open access by TopSCHOLAR®. It has been accepted for inclusion in Masters Theses & Specialist Projects by an authorized administrator of TopSCHOLAR®. For more information, please contact [topscholar@wku.edu](mailto:topscholar@wku.edu).

VISIBLE LIGHT GENERATION OF HIGH-VALENT CORROLE-MANGANESE(V)-  
OXO INTERMEDIATES AND BIOMIMETIC STUDIES OF THE OXIDATION OF  
ORGANIC SULFIDES CATALYZED BY MANGANESE CORROLES WITH  
IODOBENZENE DIACETATE

A Thesis  
Presented to  
The Faculty of the Department of Chemistry  
Western Kentucky University  
Bowling Green, Kentucky

In Partial Fulfilment  
Of the Requirements for the Degree  
Master of Science

By  
Davis Ranburger

August 2018

VISIBLE LIGHT GENERATION OF HIGH-VALENT CORROLE-MANGANESE(V)-  
OXO INTERMEDIATES AND BIOMIMETIC STUDIES OF THE OXIDATION OF  
ORGANIC SULFIDES CATALYZED BY MANGANESE CORROLES WITH  
IODOBENZENE DIACETATE

Date Recommended 07-16-2018



Dr. Rui Zhang, Director of Thesis



Dr. Darwin Dahl



Dr. Mathew Nee

Cheryl O. Davis July 27, 2018  
Dean, Graduate School Date

## ACKNOWLEDGMENTS

First and foremost, I would like to thank my advisor and mentor Dr. Rui Zhang. Throughout my years as an undergraduate student and now graduate student, Dr. Zhang has been a beacon of guidance and positivity. He has instilled his passions for life, family, and chemistry in me. I am honored to have been able to both meet and work for Dr. Zhang. I will forever remember his impact on my life for he has established a drive in me for the pursuit of lifelong learning. I could have not asked for a better advisor or teacher in my time at Western Kentucky University.

Secondly, I would like to thank my thesis committee: Dr. Darwin Dahl and Dr. Mathew Nee for their time constructive suggestions. Although I may have only had “one” advisor, I would not be where I am today had it not been for the guidance of multiple professors at WKU. In addition to Dr. Zhang and my committee members I would like to thank Dr. Kenneth Crawford for his help in my decision to pursue a career in medicine, as well as Dr. Stuart Burris as Chemistry Department Chair, Drs. Lester Pesterfield and Kevin Williams for help with NMR analysis, Dr. Eric Conte as my Graduate Coordinator and Pauline Norris of the Advanced Material Institute of WKU for help with ESI-MS data.

Third, I would like to acknowledge the past and present members of Dr. Zhang’s research lab. As for my former colleagues; Ka Wai Kwong, Wei Long Lou, Haleh Jeddi, and Ngo Fung Lee, I thank them for their direction and training. I would also like to thank my fellow lab mates who pursued their MS in my time as a graduate student: Haiyan Liu, Jonathan Malone, Dharmesh Patel, and Mike Winchester. Lastly I would like to thank the undergraduate students in our lab: Christian Alcantar, Dana Biechele-Speziale, Ben Kash,

Seth Klaine, and Ben Willis. For those moving on, good luck and I hope that they all continue to grow based on the leadership of Dr. Zhang. The friendships I have made by working in Dr. Zhang's lab are ones that will last a lifetime.

Next, I would like to recognize the importance of two chemistry staff members. Ms. Alicia Pesterfield for her phenomenal attitude and guidance for teaching labs, and for those of us who do not have family in Bowling Green, Ms. Haley Smith is who we consider to be our on-campus mother. I thank them both for their countless conversations and answers to questions that have kept me sane throughout my tenure at Western.

Furthermore, I would like to acknowledge the National Science Foundation (CHE 1464886) for financial support of this research and the WKU Office of Research for awarding me an internal FUSE grant.

Lastly and most importantly, I would like to thank my family and friends; especially my mother Melonie, father Joe, and sister Kaylee, for their endless love and support. Although my path in the future and passions for life have changed multiple times, they continue to believe in me and push me to become the best-rounded individual I can be. Thank you and I love you all.

## TABLE OF CONTENTS

### Chapter 1

Introduction.....	1
1.1 Overview of Cytochrome P450 Enzymes .....	1
1.2 Biomimetic Oxidations.....	3
1.3 High-Valent Transition Metal-Oxo Species in Catalytic Oxidations.....	5
1.4 Oxidations Catalyzed by Manganese Corroles.....	7

### Chapter 2

Experimental Section.....	9
2.1 Materials.....	9
2.2 Physical Measurements and Equipment.....	10
2.3 Methods .....	12
2.3.1 General Procedure for Photolysis of Corrole-Manganese(IV) Bromates [Mn <sup>IV</sup> (Cor)(BrO <sub>3</sub> )] and Corrole-Manganese(IV) Chlorates [Mn <sup>IV</sup> (Cor)(ClO <sub>3</sub> )].	12
2.3.2 Direct Kinetic Studies of High-Valent Metal-Oxo Intermediates.....	12
2.3.3 General Procedure for Catalytic Oxidations .....	13
2.3.4 General Procedure for Catalytic Competition Studies .....	13

2.4	Synthesis and Characterization.....	14
2.4.1	Synthesis of 5,10,15- <i>Tris</i> phenylcorrole [H <sub>3</sub> TPC] (1a).....	14
2.4.2	Synthesis of 5,10,15- <i>Tris</i> (pentafluorophenyl)corrole [H <sub>3</sub> TPFC] (1b)...	16
2.4.4	Synthesis of Corrole-Manganese(IV) Chloride [Mn <sup>IV</sup> (Cor)Cl] .....	21

### Chapter 3

	Visible Light-Induced Formation and Kinetic Studies of High-Valent Corrole-Manganese-Oxo Derivatives.....	24
3.1	Introduction .....	24
3.2	Results and Discussion .....	25
3.2.1	Generation of Corrole-Manganese(IV) Bromate Precursors [Mn <sup>IV</sup> (Cor)(BrO <sub>3</sub> )].....	25
3.2.3	Generation of Corrole-Manganese(IV) Chlorate Precursors [Mn <sup>IV</sup> (Cor)(ClO <sub>3</sub> )] .....	26
3.2.4	Visible Light Generation of Manganese(V)-Oxo Corroles.....	28
3.2.5	Kinetic Studies of High-Valent Corrole-Manganese-Oxo Species.....	31
3.2.6	A Proposed Mechanism .....	36

## Chapter 4

Oxidation of Organic Sulfides Catalyzed by Corrole-Manganese Complexes With Iodobenzene Diacetate .....	38
4.1 Introduction .....	38
4.2 Results and Discussion .....	40
4.2.1 Screening Studies in the Catalytic Oxidation of Thioanisole .....	40
4.2.2 Substrate Scope .....	43
4.2.3 Competition Studies .....	46
4.2.4 Hammett Correlation Studies .....	48
Chapter 5 .....	50
Conclusion .....	50
References .....	52
Curriculum Vitae .....	60
List of Abbreviations .....	62

## LIST OF FIGURES

Figure 1-1. (A) X-ray structure of CYP450 <sub>cam</sub> . (B) Iron protoporphyrin-IX (heme <i>b</i> ) structure.....	2
Figure 1-2. Structure of corrin, porphyrin, and corrole with each of their internal protons highlighted in red. ....	4
Figure 2-1. (A) JEOL ECA-500 MHz spectrometer. (B) Agilent 8454 diode array spectrometer. (C) SOLA SE II light engine, by Lumencor. (D) Agilent GC7820A/MS5977B. (E) Agilent 500 LCMS Ion Trap System.....	11
Figure 2-2. (A)The UV-vis spectrum of [H <sub>3</sub> TPC] ( <b>1a</b> ) in CH <sub>2</sub> Cl <sub>2</sub> ; (B) The <sup>1</sup> H-NMR spectrum of [H <sub>3</sub> TPC] ( <b>1a</b> ) in CDCl <sub>3</sub> .....	15
Figure 2-3. (A) The UV-vis spectrum of [H <sub>3</sub> TPFC] ( <b>1b</b> ) in CH <sub>2</sub> Cl <sub>2</sub> ; (B) The <sup>1</sup> H-NMR spectrum of [H <sub>3</sub> TPFC] ( <b>1b</b> ) in CDCl <sub>3</sub> ; (C) ESI-MS spectrum of [H <sub>3</sub> TPFC] ( <b>1b</b> ).17	
Figure 2-4. (A) The UV-vis spectrum of [Mn <sup>III</sup> (TPC)] ( <b>2a</b> ) in CH <sub>2</sub> Cl <sub>2</sub> ; (B) The UV-vis spectrum of [Mn <sup>III</sup> (TPFC)] ( <b>2b</b> ) in CH <sub>2</sub> Cl <sub>2</sub> ; (C) The UV-vis spectrum of [Mn <sup>III</sup> (4-NO <sub>2</sub> TPC)] ( <b>2c</b> ) in CH <sub>2</sub> Cl <sub>2</sub> . (D) ESI-MS spectrum of [Mn <sup>III</sup> (4-NO <sub>2</sub> TPC)] ( <b>2c</b> ). ..	20
Figure 2-5. (A) The UV-vis spectrum of [Mn <sup>IV</sup> (TPC)Cl] ( <b>3a</b> ) in CH <sub>2</sub> Cl <sub>2</sub> ; (B) The UV-vis spectrum of [Mn <sup>IV</sup> (TPFC)Cl] ( <b>3b</b> ) in CH <sub>2</sub> Cl <sub>2</sub> ; (C) The UV-vis spectrum of [Mn <sup>IV</sup> (4-NO <sub>2</sub> TPC)Cl] ( <b>3c</b> ) in CH <sub>2</sub> Cl <sub>2</sub> . (D) ESI-MS spectrum of [Mn <sup>IV</sup> (4-NO <sub>2</sub> TPC)Cl] ( <b>3c</b> ). .....	23

Figure 3-1. (A) UV-vis spectra of  $[\text{Mn}^{\text{IV}}(\text{TPC})\text{Cl}]$  (dashed line) and  $[\text{Mn}^{\text{IV}}(\text{TPC})(\text{BrO}_3)]$  (solid line); (B) UV-vis spectra of  $[\text{Mn}^{\text{IV}}(\text{TPFC})\text{Cl}]$  (dashed line) and  $[\text{Mn}^{\text{IV}}(\text{TPFC})(\text{BrO}_3)]$  (solid line). ..... 26

Figure 3-2. (A) UV-vis spectra of  $[\text{Mn}^{\text{IV}}(\text{TPC})\text{Cl}]$  (dashed line) and  $[\text{Mn}^{\text{IV}}(\text{TPC})(\text{ClO}_3)]$  (solid line); (B) UV-vis spectra of  $[\text{Mn}^{\text{IV}}(\text{TPFC})\text{Cl}]$  (dashed line), and  $[\text{Mn}^{\text{IV}}(\text{TPFC})(\text{ClO}_3)]$  (solid line). ..... 27

Figure 3-3. (A) Time resolved formation spectra of **6a** (red line) following visible light irradiation of **4a** ( $8.0 \times 10^{-6}$  M) over 30 s in anaerobic  $\text{CH}_3\text{CN}$  solution at 23 °C. (B) Time resolved formation spectra of **6b** (red line) following visible light irradiation of **4b** ( $7.0 \times 10^{-6}$ ) over 80 s in anaerobic  $\text{CH}_3\text{CN}$  solution at 23 °C. ... 29

Figure 3-4. (A) Time resolved formation spectra of **6a** (red line) following visible light irradiation of **5a** ( $8.0 \times 10^{-6}$ ) over 200 s in anaerobic  $\text{CH}_3\text{CN}$  solution at 23 °C. (B) Time resolved formation spectra of **6b** (red line) following visible light irradiation of **5b** ( $8.0 \times 10^{-6}$  M) over 300 s in anaerobic  $\text{CH}_3\text{CN}$  solution at 23 °C. .... 30

Figure 3-5. Chemical formation of **6b** from reaction between  $[\text{Mn}^{\text{IV}}(\text{TPFC})\text{Cl}]$  (**3b**) and  $\text{PhI}(\text{OAc})_2$  (2 equiv.) in  $\text{CH}_3\text{CN}$  over 40 s. .... 31

Figure 3-6. Time-resolved spectra of **6a** in  $\text{CH}_3\text{CN}$  reacting with thioanisole (6 mM) over 40 s. .... 32

Figure 3-7. (A) Time-resolved spectra of **6b** in  $\text{CH}_3\text{CN}$  reacting with cyclohexene (0.5 M) over 1000 s. (B) Time-resolved spectra of **6b** in  $\text{CH}_2\text{Cl}_2$  with cyclohexene (0.5 M) over 300 s. .... 33

Figure 3-8. (A) Kinetic plots of the observed rate constants ( $k_{\text{obs}}$ ) of <b>6b</b> versus the concentration of various <i>para</i> -substituted thioanisoles. (B) Hammett plot for oxidations of <i>para</i> -substituted thioanisoles with <b>6b</b> in CH <sub>3</sub> CN. ....	35
Figure 4-1. Reaction profiles for the catalytic oxidation of thioanisole with various catalyst. ....	42
Figure 4-2. Reaction profiles for the sulfoxidation of various <i>para</i> -substituted thioanisoles and sulfide substrates with <b>3a</b> as the catalyst.....	46
Figure 4-3. Hammett correlation studies ( $\log(k_{\text{rel}})$ vs $\sigma^+$ ) for Mn <sup>IV</sup> (TPC)Cl ( <b>3a</b> ) catalyzed sulfoxidation of substituted thioanisoles by PhI(OAc) <sub>2</sub> in CH <sub>3</sub> OH at 23 ± 2 °C. ....	49

## LIST OF TABLES

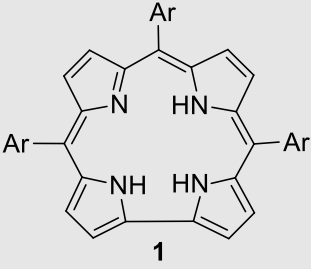
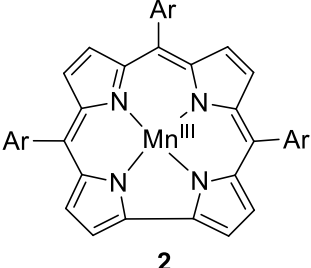
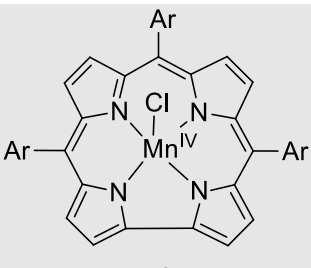
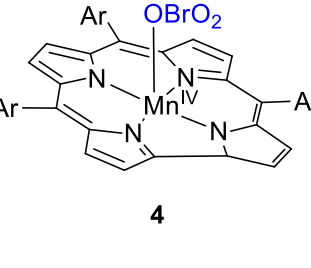
Table of Catalysts .....	xii
Table of Substrates.....	xiv
Table 1-1. Typical biomimetic oxidation reactions mediated by metalloporphyrin catalysts. .....	3
Table 3-1. Second-order rate constants for reactions with various substrates.....	34
Table 4-1. Catalytic oxidation of thioanisole by <b>2</b> and <b>3</b> with $\text{PhI}(\text{OAc})_2$ .....	41
Table 4-2. Corrole-catalyzed sulfoxidation for sulfide substrates by <b>3a</b> .....	44
Table 4-3. Relative rate constants from kinetic studies and competitive catalytic studies. .....	47

## LIST OF SCHEMES

Scheme 1-1. Hydroxylation of camphor via catalysis by CYP50 <sub>cam</sub> with molecular oxygen showing efficient selectivity of the C—H bond at position 5.....	2
Scheme 1-2. Photo-induced ligand cleavage reactions for the production of high-valent transition metal-oxo species.....	6
Scheme 1-3. Sulfoxidation of sulfides using Mn <sup>IV</sup> (TPC)Cl as the catalyst with PhI(OAc) <sub>2</sub> as the sacrificial oxidant.....	8
Scheme 2-1. Synthesis of 5,10,15- <i>Tris</i> phenylcorrole [H <sub>3</sub> TPC] ( <b>1a</b> ).....	14
Scheme 2-2. Synthesis of 5,10,15- <i>Tris</i> (pentafluorophenyl)corrole [H <sub>3</sub> TPFC] ( <b>1b</b> ) .....	16
Scheme 2-3. Synthesis of Corrole-Manganese(III) [Mn <sup>III</sup> (Cor)] ( <b>2</b> ) .....	18
Scheme 2-4. Synthesis of Corrole-Manganese(IV) Chloride [Mn <sup>IV</sup> (Cor)Cl] ( <b>3</b> ).....	21
Scheme 3-1. Axial ligand exchange from <b>3</b> to <b>4</b> with Ag(BrO <sub>3</sub> ).....	25
Scheme 3-2. Axial ligand exchange from <b>3</b> to <b>5</b> with Ag(ClO <sub>3</sub> ).....	26
Scheme 3-3. Photochemical and chemical formation of manganese(V)-oxo corroles <b>6</b> ..	28
Scheme 3-4. Two oxidation pathways for corrole-manganese(V)-oxo species, <b>6</b> controlled by the nature of the ligands and solvents.....	37
Scheme 4-1. Catalytic sulfoxidations by a variety of corrole-manganese catalysts in the presence of PhI(OAc) <sub>2</sub> and water. ....	39
Scheme 4-2. Proposed mechanism for catalytic sulfoxidation by manganese corroles with PhI(OAc) <sub>2</sub> . ....	43

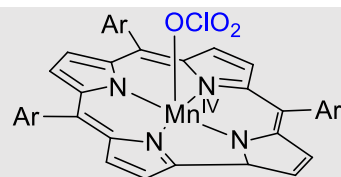
## TABLE OF NUMBERED COMPOUNDS

### Table of Catalysts

Catalyst	Name	Structure
<p><b>1a</b></p> <p><b>1b</b></p>	<p><b>TPC</b> – <i>Trisphenylcorrole</i></p> <p><b>TPFC</b> – <i>Tris(pentafluorophenyl)corrole</i></p>	 <p style="text-align: center;"><b>1</b></p>
<p><b>2</b></p>	<p><b>Mn<sup>III</sup>(Cor)</b></p> <p>Manganese(III)-corrole</p>	 <p style="text-align: center;"><b>2</b></p>
<p><b>3</b></p>	<p><b>Mn<sup>IV</sup>(Cor)Cl</b></p> <p>Manganese(IV)-corrole chloride</p>	 <p style="text-align: center;"><b>3</b></p>
<p><b>4</b></p>	<p><b>Mn<sup>IV</sup>(Cor)BrO<sub>3</sub></b></p> <p>Manganese(IV)-corrole bromate</p>	 <p style="text-align: center;"><b>4</b></p>

5

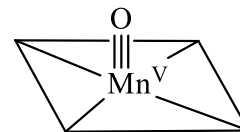
$\text{Mn}^{\text{IV}}(\text{Cor})\text{ClO}_3$   
Manganese(IV)-corrole chlorate



5

6

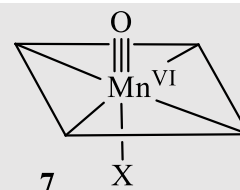
$\text{Mn}^{\text{V}}(\text{Cor})\text{O}$   
Manganese(V)-oxo corrole



6

7

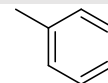
$\text{Mn}^{\text{VI}}(\text{Cor})(\text{O})(\text{X})$   
Manganese(VI)-oxo corrole



7

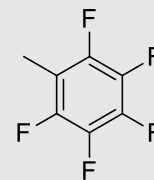
a

Ar = phenyl



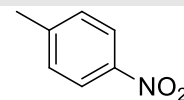
b

Ar = pentafluorophenyl



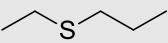
c

Ar = 4-nitrophenyl



**Table of Substrates**

Substrate	Name	Structure
8	Substrate	
9	Sulfoxide Product	
10	Sulfone Product	
a	thioanisole	<b>8a</b> 
b	4-fluorothioanisole	<b>8b</b> 
c	4-chlorothioanisole	<b>8c</b> 
d	4-methylthioanisole	<b>8d</b> 
e	4-methoxythioanisole	<b>8e</b> 
f	4-nitrothioanisole	<b>8f</b> 
g	biphenyl sulfide	<b>8g</b> 

<b>h</b>	ethyl propyl sulfide	<b>8h</b> 
<b>i</b>	1,4-oxathiane	<b>8i</b> 

---

VISIBLE LIGHT GENERATION OF HIGH-VALENT CORROLE-MANGANESE(V)-  
OXO INTERMEDIATES AND BIOMIMETIC STUDIES OF THE OXIDATION OF  
ORGANIC SULFIDES CATALYZED BY MANGANESE CORROLES WITH  
IODOBENZENE DIACETATE

Davis Ranburger

August 2018

64 Pages

Directed by: Dr. Rui Zhang, Dr. Darwin Dahl, and Dr. Mathew Nee

Department of Chemistry

Western Kentucky University

High-valent transition metal-oxo intermediates play essential roles as active oxidizing species in enzymatic and biomimetic catalytic systems. Extensive research has been conducted on a variety of transition metal catalysts being studied as models for the ubiquitous cytochrome P450 enzymes. In doing so, the production of enzyme-like oxidation catalysts and probing studies on the sophisticated oxygen atom transfer mechanism are taking place.

In this work, visible-light irradiation of highly-photo-labile corrole-manganese(IV) bromates and chlorates was studied in two corrole systems with differing electronic environments, i.e. 5,10,15-*tris*phenylcorrole ( $H_3TPC$ ) and 5,10,15-*tris*(pentafluorophenyl)corrole ( $H_3TPFC$ ). In both systems, homolytic cleavage of the O-Br and O-Cl bonds in the ligands was observed to result in one-electron photo-oxidation to afford the corrole-manganese(V)-oxo species as determined by their distinct UV-vis spectra. Kinetics of oxygen atom transfer (OAT) reactions by each photo-generated  $[Mn^V(Cor)O]$  species with various substrates were conducted in two solvents,  $CH_3CN$  and  $CH_2Cl_2$ . It was found that  $[Mn^V(Cor)O]$  exhibits noteworthy solvent and ligand effects on its reactivity and spectroscopic behavior. In the more electron-withdrawing TPFC species

in polar CH<sub>3</sub>CN solvent, Mn<sup>V</sup>-oxo corrole returned to Mn<sup>III</sup> corrole following oxidation of substrate. However, the TPFC species in the less polar CH<sub>2</sub>Cl<sub>2</sub> solvent, and in both solvents for the TPC system, Mn<sup>IV</sup> product was formed instead of Mn<sup>III</sup>. An inverted reactivity pattern, i.e. TPC > TPFC, for the Mn<sup>V</sup>-oxo corroles was observed. These spectral and kinetic results were rationalized by a multiple oxidation pathway model, where either a two-electron oxidation for oxygen atom transfer reactions takes place or a disproportionation reaction takes place forming the elusive manganese(VI)-oxo as the true oxidant. The preferred pathway is highly dependent on the nature of the corrole ligand and the solvent.

Furthermore, a variety of [Mn<sup>IV</sup>(Cor)Cl] complexes were investigated as biomimetic catalysts for the selective catalytic oxidation of the organic sulfide with mild sacrificial oxidant PhI(OAc)<sub>2</sub>. It was found that catalytic activity was affected by the oxidation state and electron environment of the catalyst. It was also found that in the same TPC system, [Mn<sup>IV</sup>(TPC)Cl] was more reactive than [Mn<sup>III</sup>(TPC)], presumably due to the Mn<sup>IV</sup>-corrole having easier access to the active metal-oxo intermediates than Mn<sup>III</sup>-corrole. In the same oxidation state, catalytic sulfoxidation of thioanisole resulted in a slower reaction rate for corrole species with more electron withdrawing ligands. In addition to thioanisole, [Mn<sup>IV</sup>(TPC)Cl] was tested for its reactivity under catalytic conditions for eight other substrates. In most cases, quantitative conversions and excellent selectivity for sulfoxide were achieved.

# CHAPTER 1

## INTRODUCTION

### 1.1 Overview of Cytochrome P450 Enzymes

Cytochrome P450 enzymes (CYP450s) were first discovered nearly 60 years ago by a group of biochemists and pharmacologists, who together studied drug metabolism.<sup>1</sup> It has been found that the CYP450s play an integral role in oxidative transformation of endogenous and/or exogenous molecules in many lifeforms including plants, bacteria, and mammals.<sup>2,3</sup> CYP450s are named for their characteristic Soret band at 450 nm when reduced and complexed with carbon monoxide.<sup>4</sup> These enzymes have two main functional roles in biological systems; one is for the metabolism of xenobiotics and the other is to aid in the biosynthesis of critical signaling molecules by acting as a catalyst.<sup>5</sup> In general, molecular oxygen is used by CYP450s for oxidation reactions, transferring one oxygen to the substrate while reducing the second to water with natural reducing agents like nicotinamide adenine dinucleotide (NADH).<sup>6</sup> Reactions mediated by CYP450s are extremely important to study in view of their characteristically high chemoselectivity, regioselectivity, and stereoselectivity.

The enzyme-catalyzed oxidation of camphor by CYP450<sub>cam</sub> is one of the most distinct examples for a stereospecific, chemospecific, and regiospecific oxidation.<sup>7</sup> CYP450<sub>cam</sub> was found by Gunsulas and colleagues in *Pseudomonas putida*, a species of bacterium that is known for its ability to metabolize certain substrates including camphor, caffeine, and benzene.<sup>8</sup> The X-ray crystallography structure and figure of its iron-protoporphyrin-IX active site of CYP450<sub>cam</sub> can be found in Fig. 1-1. Its ability to

metabolize substrates is typically attributed to its CYP450 monooxygenases.<sup>8</sup> CYP450<sub>cam</sub> hydroxylates camphor specifically to 5-*exo*-hydroxycamphor as outlined in Scheme 1-1.

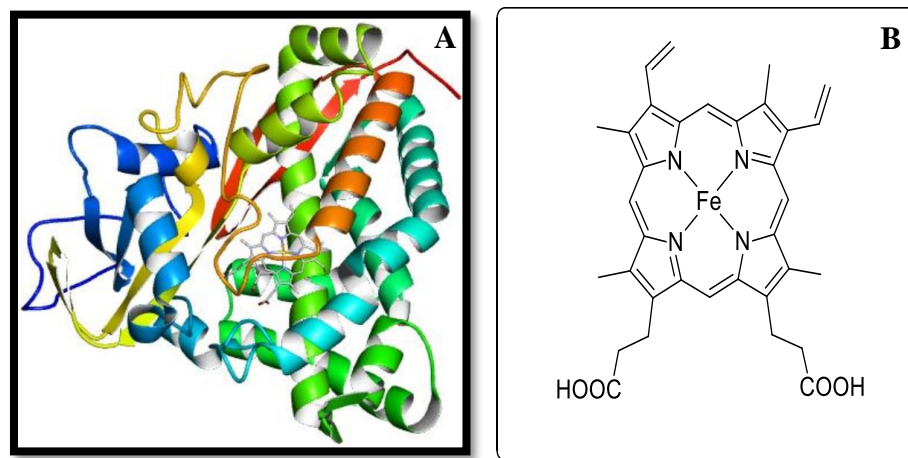
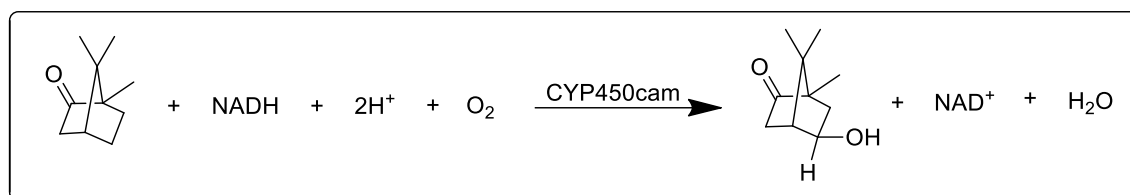


**Figure 1-1.** (A) X-ray structure of CYP450<sub>cam</sub>.<sup>7</sup> (B) Iron protoporphyrin-IX (heme *b*) structure.

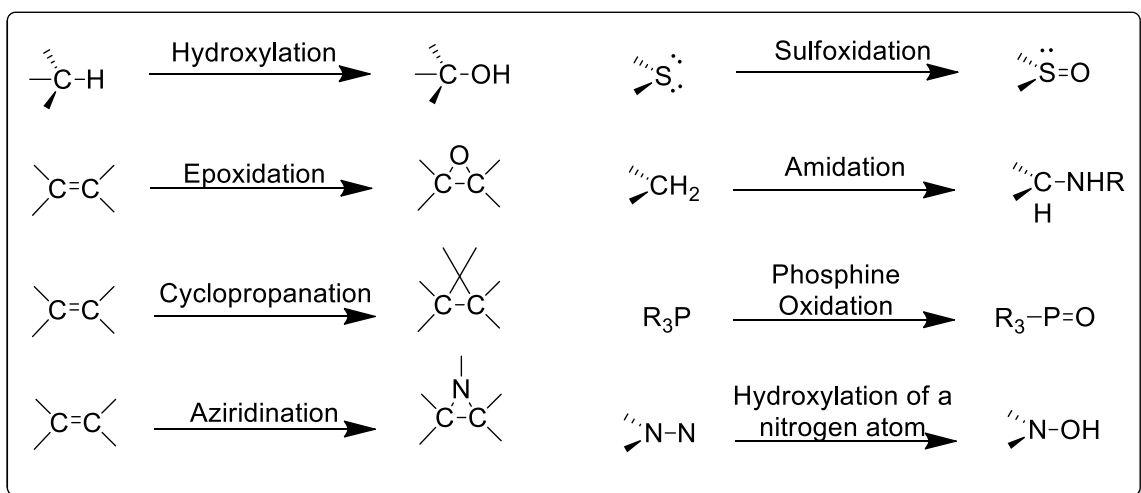


**Scheme 1-1.** Hydroxylation of camphor via catalysis by CYP50<sub>cam</sub> with molecular oxygen showing efficient selectivity of the C—H bond at position 5.

## 1.2 Biomimetic Oxidations

In biomimetic oxidation, a high-valent metal-oxo species is formed via oxidation of a transition metal catalyst by a sacrificial oxidant. Then, the metal-oxo intermediate oxidizes available substrates.<sup>9,10</sup> To study this sophisticated oxidation mechanism, many transition metal catalysts have been synthesized as models that resemble CYP450 enzymes.<sup>11</sup> The most extensively studied biomimetic catalysts are metalloporphyrins, which closely resemble the active site of CYP450 enzymes for a variety of oxidation reactions (Table 1-1).

**Table 1-1.** Typical biomimetic oxidation reactions mediated by metalloporphyrin catalysts.



Closely related to porphyrins are corroles and corrins (Fig. 1-2). One main difference between the three is the number of available ionizable protons in their N<sub>4</sub> coordination core. As seen in Fig. 1-2, corrins have one internal proton, porphyrins have

two (dianionic), and corroles have three (trianionic).<sup>12</sup> Corroles have a similar backbone to that of corrins, the core structure of vitamin B<sup>12</sup>, but the difference between porphyrins and corroles is extremely important for their role in transition-metal-oxo chemistry because having three internal ionizable protons in corroles allows for the coordination of higher oxidation-state transition metals.

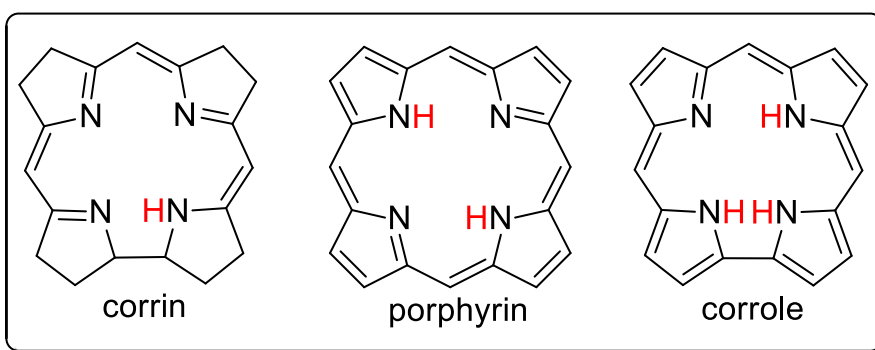


**Figure 1-2.** Structure of corrin, porphyrin, and corrole with each of their internal protons highlighted in red.

Recently, interest has grown in the catalytic properties of the 19-membered corroles due to their capacity to access and stabilize higher oxidation state metal-oxo species.<sup>13-16</sup> Corrole synthesis was first reported in 1965 by Johnson and coworkers.<sup>17</sup> It was not until 1999 that Gross and colleagues reported a new synthetic technique for the solvent-free condensation of pyrrole and aldehydes.<sup>18</sup> Furthermore, Gross went on to report the first application of metallocorroles for the catalytic cyclopropanation, epoxidation, and hydroxylation in the presence of iodosylbenzene and carbenoid oxidants. In comparison to porphyrin systems, the  $\pi$ -electron-system of corroles is far more electron rich than that of

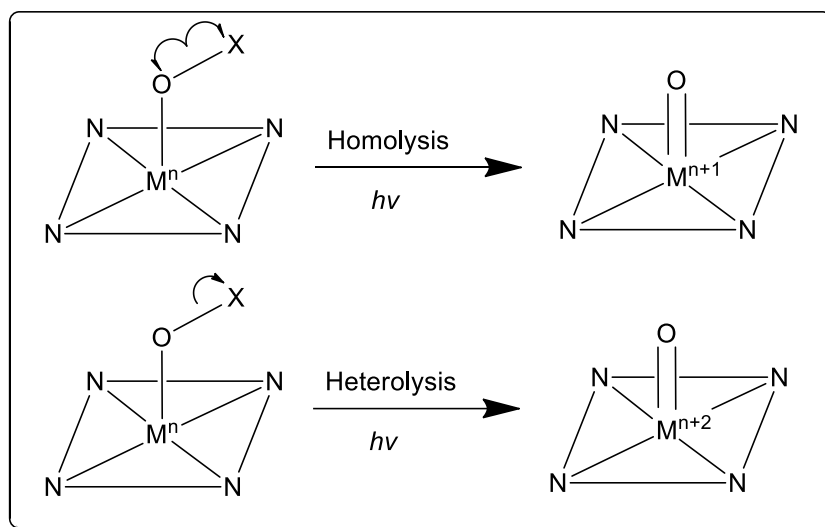
porphyrins, allowing for these unusually high oxidation state transition metals.<sup>19</sup> Thus, when complexed with manganese, for example, the corrole systems have a natural tendency to support manganese(V)-oxo species while porphyrins favor the manganese(IV)-oxo state.

### **1.3 High-Valent Transition Metal-Oxo Species in Catalytic Oxidations**

The study of the catalytic oxidations of high-valent metal-oxo species has grown in significant interest due to their involvement in the catalytic cycle of CYP450s. These high-valent metal-oxo species are typically thought to be the active oxidizing species for metallo-porphyrin mediated catalysis.<sup>20</sup> Prior to 1980, when Groves et al. reported the first high-valent metal-oxo species, only iron had been used due to its relation to the protoporphyrin-IX heme active site of CYP450s.<sup>21</sup> This opened the door for the development of metalloporphyrins with a variety of transition metals other than iron. This same concept has been applied in corrole systems.

Photochemistry has proven to be particularly fascinating in the exploration of metal-oxo chemistry.<sup>22</sup> Photochemical catalysis is also essential to develop greener methods because the activation of the catalyst is obtained through absorption of a photon, leaving no residue. This is principally important because most chemical methods involve the use of toxic or polluting reagents.<sup>23</sup> Thus, the use of visible light to activate reversible redox processes of the metal centers in catalysts could avoid the disadvantages that arise when using chemical reagents.<sup>24</sup> Newcomb and coworker were the first to develop photo-induced ligand cleavage reactions to photochemically generate a variety of high-valent transition metal-oxo derivatives supported by porphyrin and corrole ligands.<sup>25-27</sup> As shown

in Scheme 1-2, the precursor complexes are coordinated with a metal of  $n$  oxidation state that is bound to an oxygen containing ligand. Photolysis proceeds in one of two pathways: homolytic cleavage of the O-X bond in the ligand resulting in an  $n + 1$  oxidation state metal-oxo species or through heterolytic cleavage of the same bond resulting in an  $n + 2$  oxidation state metal-oxo species.



**Scheme 1-2.** Photo-induced ligand cleavage reactions for the production of high-valent transition metal-oxo species.

The photochemical approach produces metal-oxo species basically instantaneously. This allows for their detection and kinetic studies of their oxidations to be analyzed on much shorter timescales than the fastest mixing experiments. Of the many species tested, those containing manganese as the metal are among the more reactive transition metal-oxo derivatives. In Chapter 3, it is shown that visible-light irradiation of photo-labile bromate and chlorate manganese(IV)-corrole precursors gave the corresponding high-valent manganese(V)-oxo corroles. Meanwhile, the kinetic studies of these photo-generated

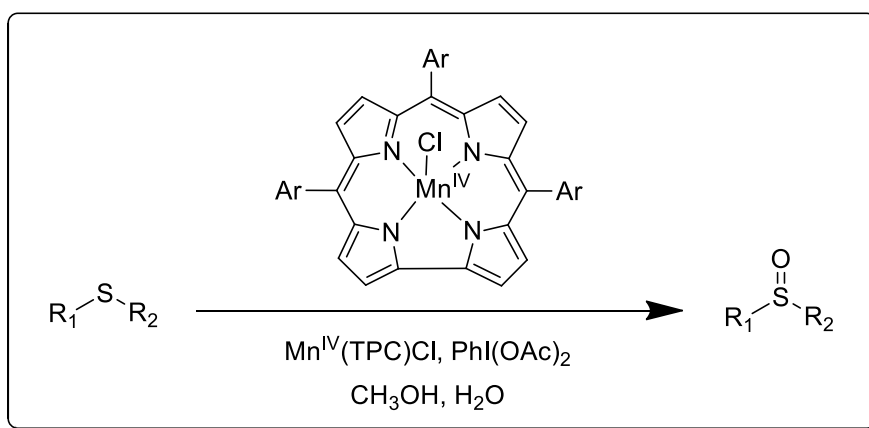
metal-oxo species also provide insights into high-valent species to propose their mechanism of oxidation.

#### **1.4 Oxidations Catalyzed by Manganese Corroles**

In the pharmaceutical industry, selective oxidation of sulfides to sulfoxides, without over-oxidation to sulfones, is extremely important.<sup>28</sup> Currently, sulfoxides are in use for the formulation of both antibacterial and antifungal compounds.<sup>29</sup> Orthodox and outdated methods of sulfoxidation involve strong oxidizing agents including peroxyacids and toxic heavy metal catalyst that have proven to be detrimental for the environment.<sup>30,31</sup> Therefore, the need for greener, environmentally-conscience sulfoxidation catalysts is exceedingly apparent for the future.<sup>32</sup>

As previously reported, manganese porphyrins and corroles act as efficient catalysts for sulfoxidation reactions.<sup>33</sup> While manganese porphyrin complexes exhibit high conversion rates, they lack selectivity, allowing for the over-oxidation of substrate.<sup>34</sup> Conversely, manganese corroles have an enhanced ability to selectively oxidize substrate with minimal over-oxidative product formation coupled with a slower rate of conversion.<sup>35</sup> There is room for improvement, in both cases, which is the driving force behind catalytic sulfoxidation testing in this work. Throughout the pharmaceutical industry, there exists a high demand for efficiently selective, versatile catalysts for the sulfoxidation of substrates with high product selectivity at an effective conversion rate under mild oxidative conditions.

The 19-carbon, fully conjugated, and aromatic corroles differ in their stability compared to porphyrins due to their susceptibility to thermal degradation.<sup>36</sup> However, their high-valent metal complexes show considerably higher stability than those of porphyrin, due to the trianionic nature of the corrole ligands.<sup>37</sup> Metallocorroles have been used for many biochemical applications including anticancer agents<sup>38-43</sup>, antioxidant therapy<sup>44,45</sup>, and in diabetic therapy.<sup>46</sup> The first report for the utilization of metallocorroles in catalysis was in 2000 where iron(III) corrole was employed as the catalyst for cyclopropanation and epoxidation reactions with iodosylbenzene as an oxygen source.<sup>47</sup> In Chapter 4, an emphasis on the sulfoxidation of various sulfides is investigated under catalytic conditions with manganese(IV)-chloride 5, 10, 15-*tris*phenylcorrole [ $\text{Mn}^{\text{IV}}(\text{TPC})\text{Cl}$ ] and iodobenzene diacetate as a mild oxidant (Scheme 1-3).



**Scheme 1-3.** Sulfoxidation of sulfides using  $\text{Mn}^{\text{IV}}(\text{TPC})\text{Cl}$  as the catalyst with  $\text{PhI}(\text{OAc})_2$  as the sacrificial oxidant.

# CHAPTER 2

## EXPERIMENTAL SECTION

### 2.1 Materials

All commercial reagents were of the best available purity and used as supplied unless otherwise specified. All organic solvents used for synthesis and purification, including acetone, acetonitrile, benzene, chloroform, dichloromethane, diethyl ether, ethanol, methanol, hexane, and *N,N*-dimethylformamide (DMF) were purchased from Sigma-Aldrich Chemical Company. Pyrrole was freshly distilled for use in synthesis. Benzaldehyde, hydrochloric acid (HCl), boron trifluoride diethyl etherate (BF<sub>3</sub>·Et<sub>2</sub>O), tetrachloro-1,4-benzoquinone (*p*-chloranil), 2,3-dichloro-5,6-dicyano-*p*-benzoquinone (DDQ), basic alumina [Al<sub>2</sub>O<sub>3</sub>] with an activity of one manganese(II) acetate tetrahydrate, chloroform-*d*, iodobenzene diacetate [PhI(OAc)<sub>2</sub>], *tris*-(4-bromophenyl)ammoniumyl hexachloroantimonate [(4-BrC<sub>5</sub>H<sub>4</sub>)<sub>3</sub>N]SbCl<sub>6</sub>, 5,10,15-*tris*(pentafluorophenyl)corrole [H<sub>3</sub>TPFC], and 5,10,15-*tris*(4-nitrophenyl)corrole [H<sub>3</sub>(4-NO<sub>2</sub>)TPC] were purchased from Sigma-Aldrich Chemical Company and used as such. Substrates used for kinetic studies were purified by silica gel column prior to use including cyclohexene, *cis*-cyclooctene, ethyl benzene, styrene, thioanisole, 4-fluorothioanisole, 4-chlorothioanisole, 4-methylthioanisole, and 4-methoxythioanisole. Substrates for catalytic oxidations were purchased and used as such, including the prior listed thioanisole substrates, 4-nitrothioanisole, diphenyl sulfide, ethyl propyl sulfide, and 1,4-oxathiane. All bromate, and chlorate precursors of metallocorrole complexes were prepared *in situ* by stirring with excess silver bromate Ag(BrO<sub>3</sub>) and silver chlorate Ag(ClO<sub>3</sub>) with [Mn<sup>III</sup>(Cor)] as described later in Chapter 2.

## 2.2 Physical Measurements and Equipment

<sup>1</sup>H-NMR analysis was performed on a JEOL ECA-500 MHz spectrometer (Fig. 2-1 A) at 298K with tetramethylsilane (TMS) as the internal standard with deuterated chloroform (CDCl<sub>3</sub>) as the solvent. Chemical shifts (ppm) were reported relative to the standard TMS peak. UV-Vis spectra were conducted on an Agilent 8454 diode array spectrometer (Fig. 2-1 B) using standard 1.0-cm quartz cuvettes. Visible light was produced by a SOLA SE II light engine (by Lumencor) fitted with a liquid light guide and output power that could be adjusted from 6-120 W (Fig. 2-1 C). Gas chromatography-mass spectrometry (GC-MS) analysis were performed on an Agilent GC7820A/MS5977B (Fig. 2-1 D), coupled with an auto sample injector using an Agilent DB-5 capillary column. Electrospray ionization-mass spectroscopy (ESI-MS) data was collected using an Agilent 500 LCMS Ion Trap System (Fig. 2-1 E).



**Figure 2-1.** (A) JEOL ECA-500 MHz spectrometer. (B) Agilent 8454 diode array spectrometer. (C) SOLA SE II light engine, by Lumencor. (D) Agilent GC7820A/MS5977B. (E) Agilent 500 LCMS Ion Trap System.

## 2.3 Methods

### 2.3.1 General Procedure for Photolysis of Corrole-Manganese(IV) Bromates

#### [Mn<sup>IV</sup>(Cor)(BrO<sub>3</sub>)] and Corrole-Manganese(IV) Chlorates [Mn<sup>IV</sup>(Cor)(ClO<sub>3</sub>)]

Manganese(IV) corrole complexes [Mn<sup>IV</sup>(Cor)Cl] were stirred in anaerobic CH<sub>3</sub>CN with an excess of a silver salts [Ag(BrO<sub>3</sub>), Ag(ClO<sub>3</sub>)] used for the facile exchange of the chloride counter ions in the corrole complexes, resulting in the formation of the photo-labile bromate [Mn<sup>IV</sup>(Cor)(BrO<sub>3</sub>)] or chlorate [Mn<sup>IV</sup>(Cor)(ClO<sub>3</sub>)] products. The expected AgCl precipitate formed as a result of the exchange. The exchange reactions were monitored respectively by UV-vis spectroscopy. Immediately following this conversion, the complexes were used for photochemical studies.

### 2.3.2 Direct Kinetic Studies of High-Valet Metal-Oxo Intermediates

Following the formation of the high-valent metal-oxo species with an excess amount of organic substrate (> 100 equiv.) were conducted in multiple solvents (2 mL) at 23 ± 2 °C. The photo-generated [Mn<sup>V</sup>(Cor)O] approximate concentrations were estimated assuming the 100% conversion of from the manganese(IV) precursors prior to photochemical reactions. The rates of reaction, representing the rate at which the oxo group transfers from the [Mn<sup>V</sup>(Cor)O] to the available substrate were monitored via the decay of the Soret absorption band of the manganese(V)-oxo species. The data resulted in pseudo-first-order observed rate constants, i.e.  $k_{\text{obs}}$ . Plots of these values against the concentrations of substrates were linear in all cases.

The second-order rate constants for the reaction of the manganese(V)-oxo species with substrates, were then solved according to

$$k_{\text{obs}} = k_{\text{o}} + k_{\text{ox}}[\text{Sub}] \quad \text{Eq. 1,}$$

where  $k_{\text{obs}}$  is the observed rate constant,  $k_{\text{o}}$  is the background decay rate constant determined without substrate,  $k_{\text{ox}}$  is the second-order rate constant for the reaction with substrate, and [Sub] is the concentration of substrate. By plotting  $k_{\text{obs}}$  versus the concentration of substrate, the slope of the line-of-best-fit will be the second-order rate constant value.

### 2.3.3 General Procedure for Catalytic Oxidations

The corrole-manganese complexes were investigated as catalysts for oxidation of a variety of organic sulfides, including six *para*-substituted thioanisoles along with three other sulfide compounds. Reactions were conducted in methanol solution (2 mL) which contains catalyst (1  $\mu\text{mol}$ ), a small amount of water (4.5  $\mu\text{L}$ ), organic substrate (0.5 mmol), and 1.5 equiv. of  $\text{PhI}(\text{OAc})_2$  (0.75 mmol) as the sacrificial oxidant. Aliquots of the reactions were analyzed by GC-MS and/or  $^1\text{H}$  NMR to determine the conversion of substrates and product selectivity. Studies of the effects of catalyst, oxidant concentrations, and catalytic competition studies were conducted in a similar fashion.

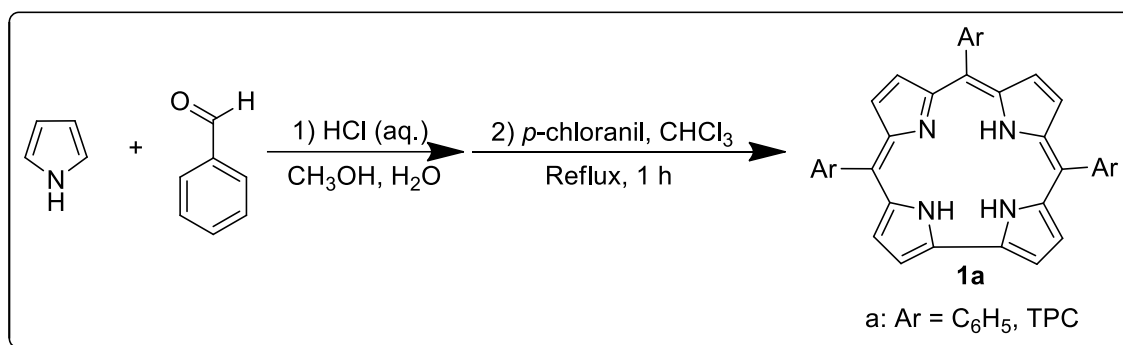
### 2.3.4 General Procedure for Catalytic Competition Studies

In competition studies, a methanol solution was made containing manganese(IV) corrole catalyst (1  $\mu\text{mol}$ ), a small amount of water (4.5  $\mu\text{L}$ ),  $\text{PhI}(\text{OAc})_2$  (0.1 mmol) as the

limiting reagent, and equal amounts of two substrates, e.g. thioanisole (0.25 mmol) and a *para*-substituted thioanisole (0.25 mmol). Relative rate ratios for catalytic oxidation were determined by GC based on the relative amounts of each sulfoxide product formed. The ratio of product formation should directly reflect the relative sulfide reactivity toward corrole-manganese-catalyzed oxidation.

## 2.4 Synthesis and Characterization

### 2.4.1 Synthesis of 5,10,15-*Trisphenylcorrole* [ $H_3TPC$ ] (**1a**)



#### Scheme 2-1. Synthesis of 5,10,15-*trisphenylcorrole* [ $H_3TPC$ ] (**1a**)

The synthesis of 5,10,15-trisphenylcorrole (**1a**) was conducted based on reported methods (Scheme 2-1).<sup>22</sup> The first step allows for an acidic environment to aid in the nucleophilic addition between pyrrole and benzaldehyde. The second step results in the corrole ring closure via a one-step oxidation with *p*-chloranil. Freshly distilled pyrrole (10 mmol) and benzaldehyde (5 mmol) were joined in a solution consisting of a water/methanol mixture (1:1). Hydrochloric acid (HCl, 0.12 M) was added as the acid catalyst for the condensation to occur and the resulting solution was stirred at room temperature for 3 h. The product of the first step was then extracted using chloroform (CHCl<sub>3</sub>) and washed with

water twice. The resulting mixture was dried with anhydrous sodium sulfate. The filtered solution was diluted with  $\text{CHCl}_3$  (300 mL) and refluxed for 1 h with excess *p*-chloranil. Column chromatography (silica gel) was then conducted with dichloromethane/hexane solution as the eluent, which afforded pure corrole product. The structure of the product was confirmed by UV-vis spectroscopy (Fig. 2-2 A),  $^1\text{H-NMR}$  (Fig. 2-2 B) and ESI-MS.

**Yield** = 220 mg (25%)

**UV-vis** ( $\text{CH}_2\text{Cl}_2$ )  $\lambda_{\text{max}}/\text{nm}$ : 415 (Soret), 570, 615, 647

**$^1\text{H-NMR}$**  (500 MHz,  $\text{CDCl}_3$ ):  $\delta$ , ppm: 7.73-7.83 (m, 9H), 8.17 (d, 2H), 8.38 (d, 4H), 8.55 (2 2H), 8.60 (d, 2H), 8.87 (d, 2H), 8.95 (d, 2H)

**ESI-MS**:  $m/z$ : 527.3  $[\text{M}]^+$

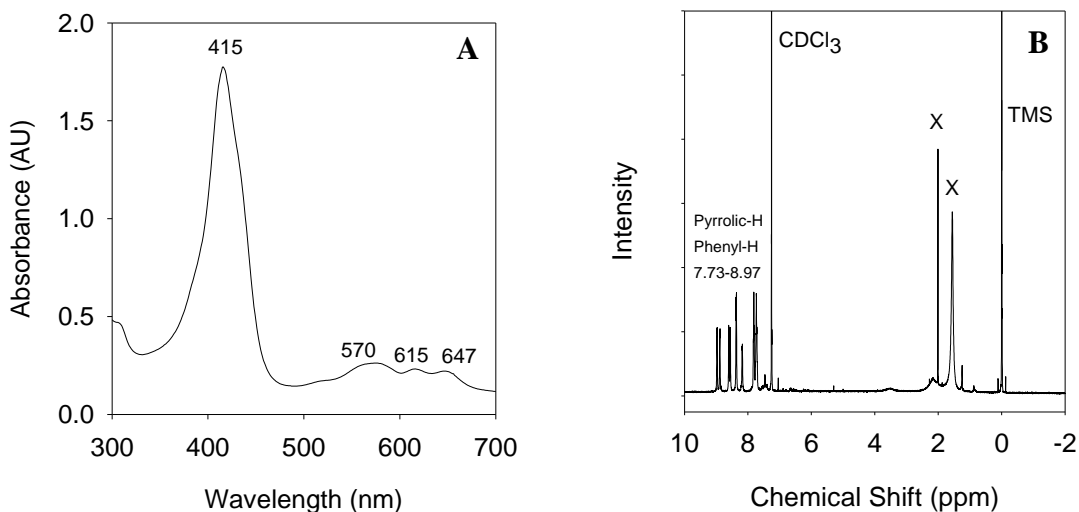
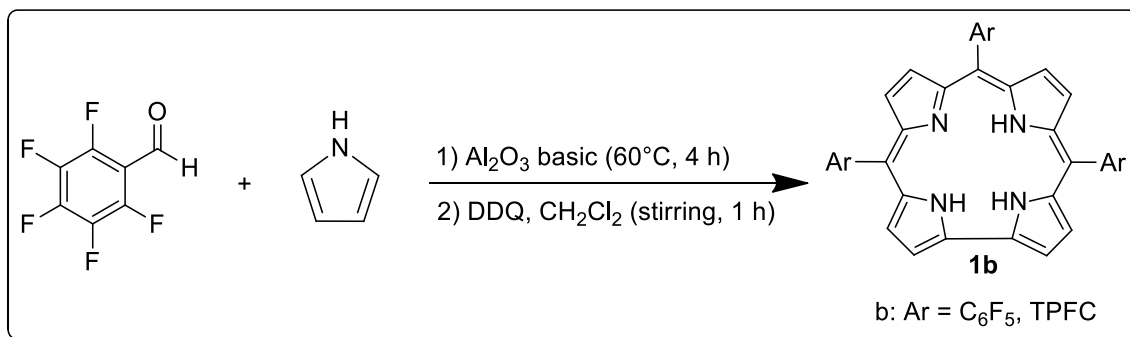


**Figure 2-2.** (A) The UV-vis spectrum of  $[\text{H}_3\text{TPC}]$  (**1a**) in  $\text{CH}_2\text{Cl}_2$ ; (B) The  $^1\text{H-NMR}$  spectrum of  $[\text{H}_3\text{TPC}]$  (**1a**) in  $\text{CDCl}_3$

## 2.4.2 Synthesis of 5,10,15- *Tris*(pentafluorophenyl)corrole [H<sub>3</sub>TPFC] (**1b**)



**Scheme 2-2.** Synthesis of 5,10,15-*tris*(pentafluorophenyl)corrole [H<sub>3</sub>TPFC] (**1b**)

5,10,15-*Tris*(pentafluorophenyl)corrole (**1b**) was synthesized using the methods (Scheme 2-2) reported by Gross and colleagues.<sup>18</sup> First, a one-to-one molar ratio of pentafluorobenzaldehyde and freshly distilled pyrrole (15 mmol) was dissolved in CH<sub>2</sub>Cl<sub>2</sub>. This solvent-free step of the reaction was conducted on a solid support of alumina (Al<sub>2</sub>O<sub>3</sub>, 3 g) and heated to 100 °C for 4 h. The expected condensation reaction then takes place once all of the solvent is evaporated. Then, 2,3-dichloro-5,6-dicyanobenzoquinone (DDQ) was added to the tarry mixture as an oxidant. TLC was used to monitor reaction progress. A UV lamp was used to identify the formation of product on the TLC plates due to the fluorescent properties of the ligand. A silica gel column was then performed with dichloromethane/hexane solutions as the eluent. The pure corrole was characterized by UV-vis spectroscopy (Fig. 2-3 A), <sup>1</sup>H-NMR spectra (Fig. 2-3 B), and ESI-MS (Fig. 2-3 C).

**Yield** = 145 mg (5%)

**UV-vis** (CH<sub>2</sub>Cl<sub>2</sub>) λ<sub>max</sub>/nm: 407 (Soret), 561, 604

**<sup>1</sup>H-NMR** (500 MHz, CDCl<sub>3</sub>): δ, ppm: 8.57 (d, 4H), 8.75 (d, 2H), 9.10 (d, 2H)

**ESI-MS:** *m/z*: 797.27 [M]<sup>+</sup>

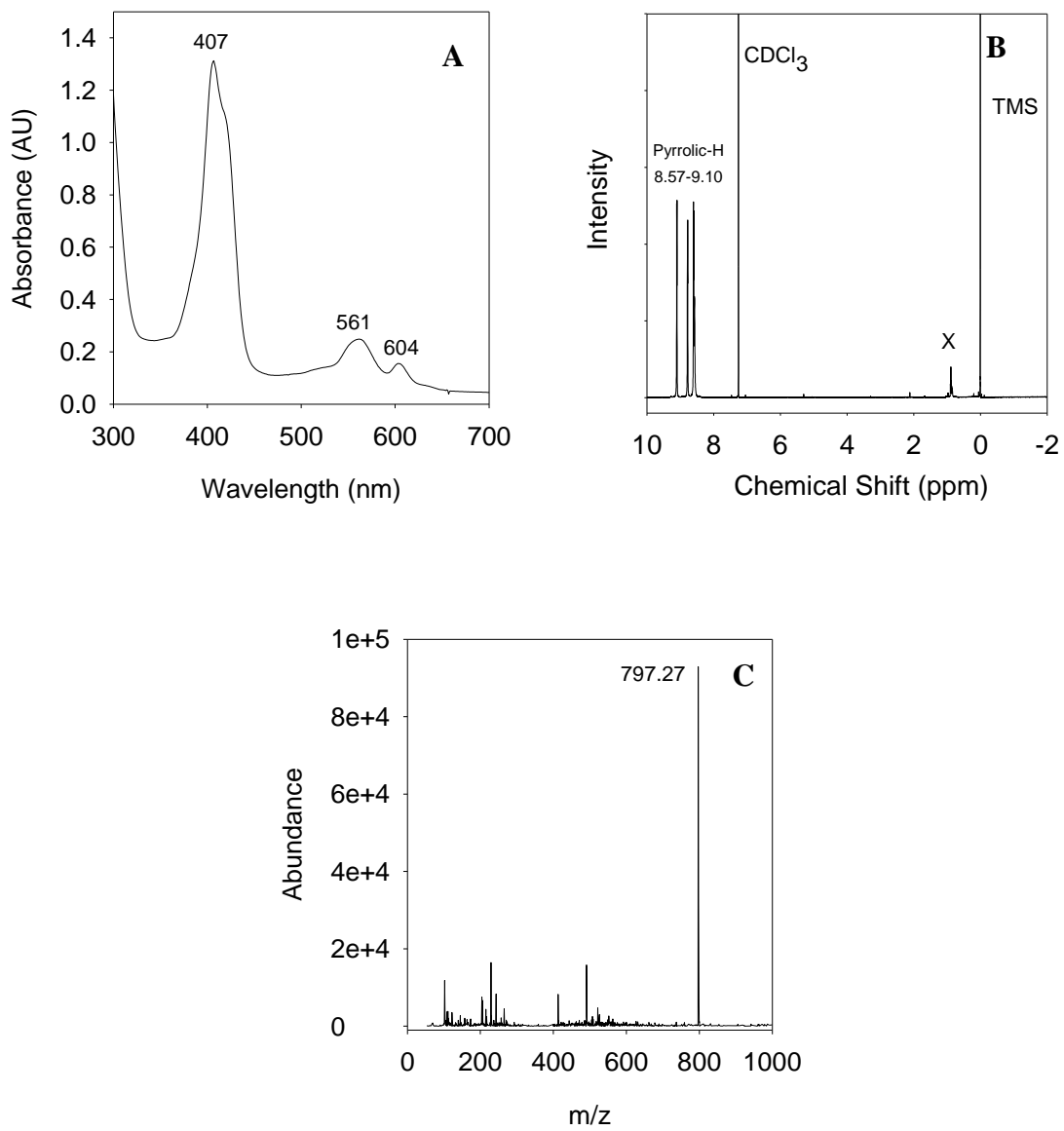
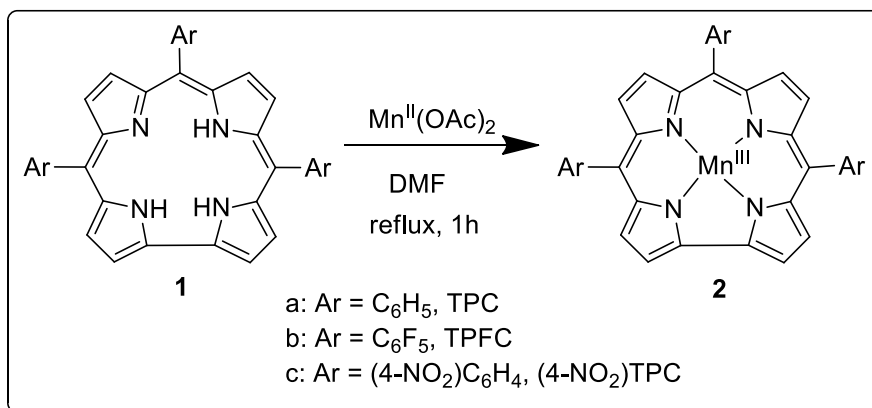


**Figure 2-3.** (A) The UV-vis spectrum of [H<sub>3</sub>TPFC] (**1b**) in CH<sub>2</sub>Cl<sub>2</sub>; (B) The <sup>1</sup>H-NMR spectrum of [H<sub>3</sub>TPFC] (**1b**) in CDCl<sub>3</sub>; (C) ESI-MS spectrum of [H<sub>3</sub>TPFC] (**1b**).

### 2.4.3 Synthesis of Corrole-Manganese(III) [Mn<sup>III</sup>(Cor)]



**Scheme 2-3.** Synthesis of Corrole-Manganese(III) [Mn<sup>III</sup>(Cor)] (2)

Metalation of corrole complexes was performed based on the methods defined by Simikhovich et al.<sup>47</sup> Each corrole ligand (100 mg) was dissolved in DMF (30 mL) in a round bottom flask. The mixture was degassed with argon for approximately 5 min. A large excess of manganese(II) acetate tetrahydrate (~300 mg) was added and the mixture was refluxed for 30-60 min (Scheme 2-3). The conversion was monitored by TLC analysis. DMF was then evaporated via rotary evaporation under vacuum. The crude solid was dissolved in diethyl ether and purified on a silica gel column with diethyl ether to afford the expected manganese corrole complexes. The purified products were characterized by UV-vis (Fig. 2-4 A, 2-4 B, 2-4 C), and ESI-MS, represented by the spectrum for [Mn<sup>III</sup>(4-NO<sub>2</sub>TPC)] (Fig. 2-4 D).

**Mn<sup>III</sup>(TPC) [2a]**

**Yield** = 81 mg (70%)

**UV-vis** (CH<sub>2</sub>Cl<sub>2</sub>)  $\lambda_{\text{max}}$ /nm: 403, 431, 651

**ESI-MS:**  $m/z$ : 578.21 [M]<sup>+</sup>

**Mn<sup>III</sup>(TPFC) [2b]**

**Yield** = 97 mg (87%)

**UV-vis** (CH<sub>2</sub>Cl<sub>2</sub>)  $\lambda_{\text{max}}$ /nm: 400, 415, 469, 598

**ESI-MS:**  $m/z$ : 848.19 [M]<sup>+</sup>

**Mn<sup>III</sup>(4-NO<sub>2</sub>TPC) [2c]**

**Yield** = 33 mg (31%)

**UV-vis** (CH<sub>3</sub>CN)  $\lambda_{\text{max}}$ /nm: 428, 480, 658

**ESI-MS:**  $m/z$ : 713.1 [M]<sup>+</sup>

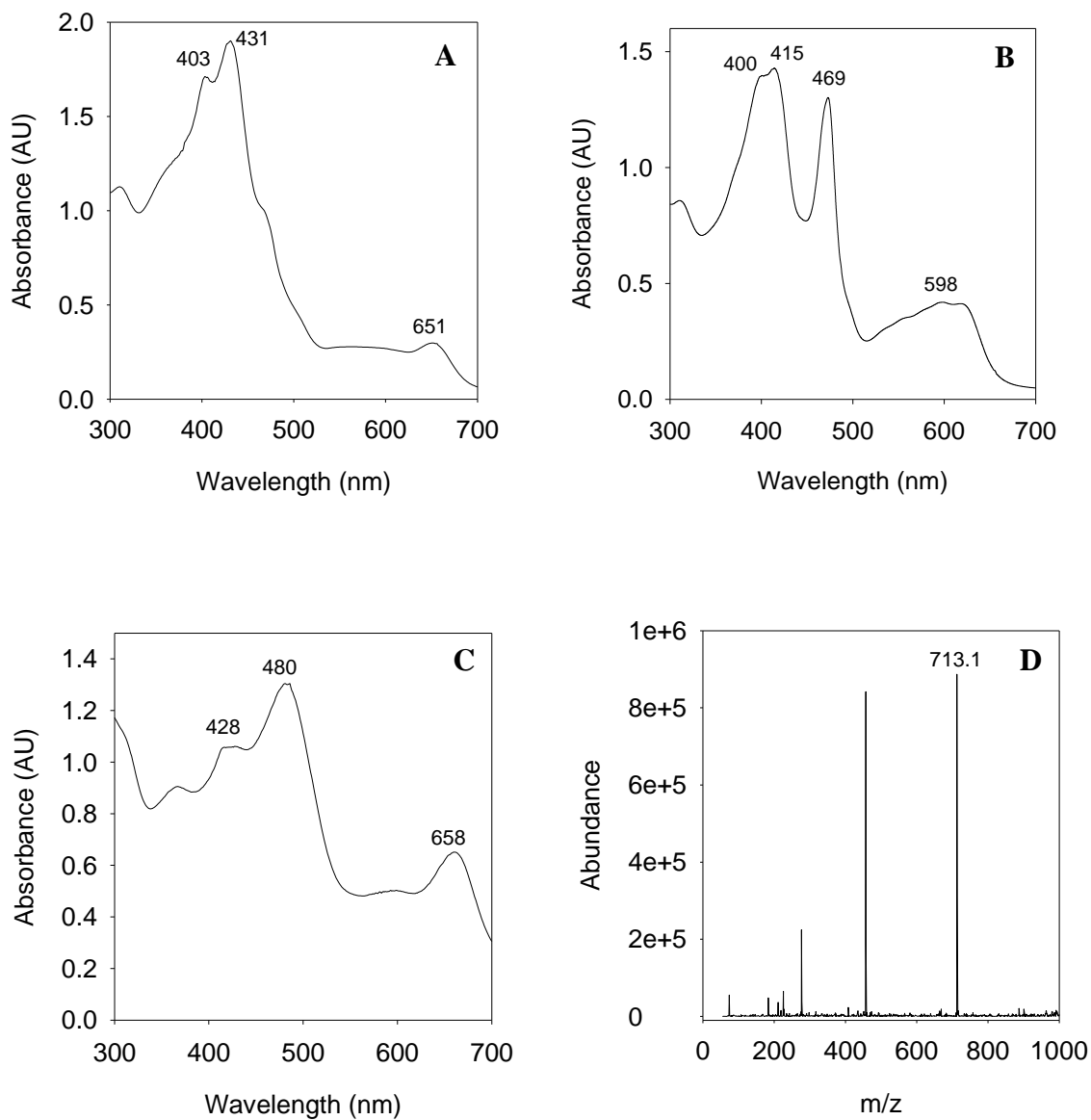
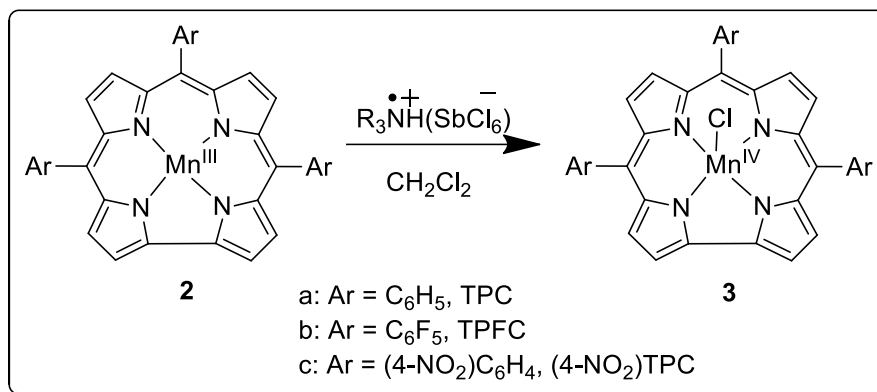


**Figure 2-4.** (A) The UV-vis spectrum of [Mn<sup>III</sup>(TPC)] (**2a**) in CH<sub>2</sub>Cl<sub>2</sub>; (B) The UV-vis spectrum of [Mn<sup>III</sup>(TPFC)] (**2b**) in CH<sub>2</sub>Cl<sub>2</sub>; (C) The UV-vis spectrum of [Mn<sup>III</sup>(4-NO<sub>2</sub>TPC)] (**2c**) in CH<sub>2</sub>Cl<sub>2</sub>. (D) ESI-MS spectrum of [Mn<sup>III</sup>(4-NO<sub>2</sub>TPC)] (**2c**).

#### 2.4.4 Synthesis of Corrole-Manganese(IV) Chloride [Mn<sup>IV</sup>(Cor)Cl]



**Scheme 2-4.** Synthesis of Corrole-Manganese(IV) Chloride [Mn<sup>IV</sup>(Cor)Cl] (**3**)

According to previous studies, the treatment of the corrole-manganese(III) complexes, **2**, with *tris*(4-bromophenyl)ammoniumyl hexachloroantimonate (1:1 ratio by mass) that functions as a one-electron oxidant and as the counter anion donor in CH<sub>2</sub>Cl<sub>2</sub> (Scheme 2-4), affords the respective corrole-manganese(IV) chloride species, **3**.<sup>14</sup> The resulting compound was then purified by silica gel column chromatography with CH<sub>2</sub>Cl<sub>2</sub> as the eluent to give the expected product. UV-vis spectroscopy (Fig. 2-5 A, 2-5 B, 2-5 C) and ESI-MS, represented by the spectrum for [Mn<sup>IV</sup>(4-NO<sub>2</sub>TPC)Cl] (Fig. 2-5 D), were used to confirm the manganese(IV) corrole product.

**Mn<sup>IV</sup>(TPC)Cl [3a]**

**Yield** = 73 mg (90%)

**UV-vis** (CH<sub>2</sub>Cl<sub>2</sub>)  $\lambda_{\text{max}}$ /nm: 430, 603

**ESI-MS:**  $m/z$ : 578.11 [M]<sup>+</sup>, 613.05 [M – Cl]<sup>+</sup>

**Mn<sup>IV</sup>(TPFC)Cl [3b]**

**Yield** = 75 mg (89%)

**UV-vis** (CH<sub>2</sub>Cl<sub>2</sub>)  $\lambda_{\text{max}}$ /nm: 361, 416, 593

**ESI-MS:**  $m/z$ : 848.19 [M]<sup>+</sup>, 884.05 [M – Cl]<sup>+</sup>

**Mn<sup>IV</sup>(4-NO<sub>2</sub>TPC)Cl [3c]**

**Yield** = 5.7 mg (36%)

**UV-vis** (CH<sub>2</sub>Cl<sub>2</sub>)  $\lambda_{\text{max}}$ /nm: 363, 424, 602

**ESI-MS:**  $m/z$ : 746.99 [M]<sup>+</sup>, 713.15 [M – Cl]<sup>+</sup>

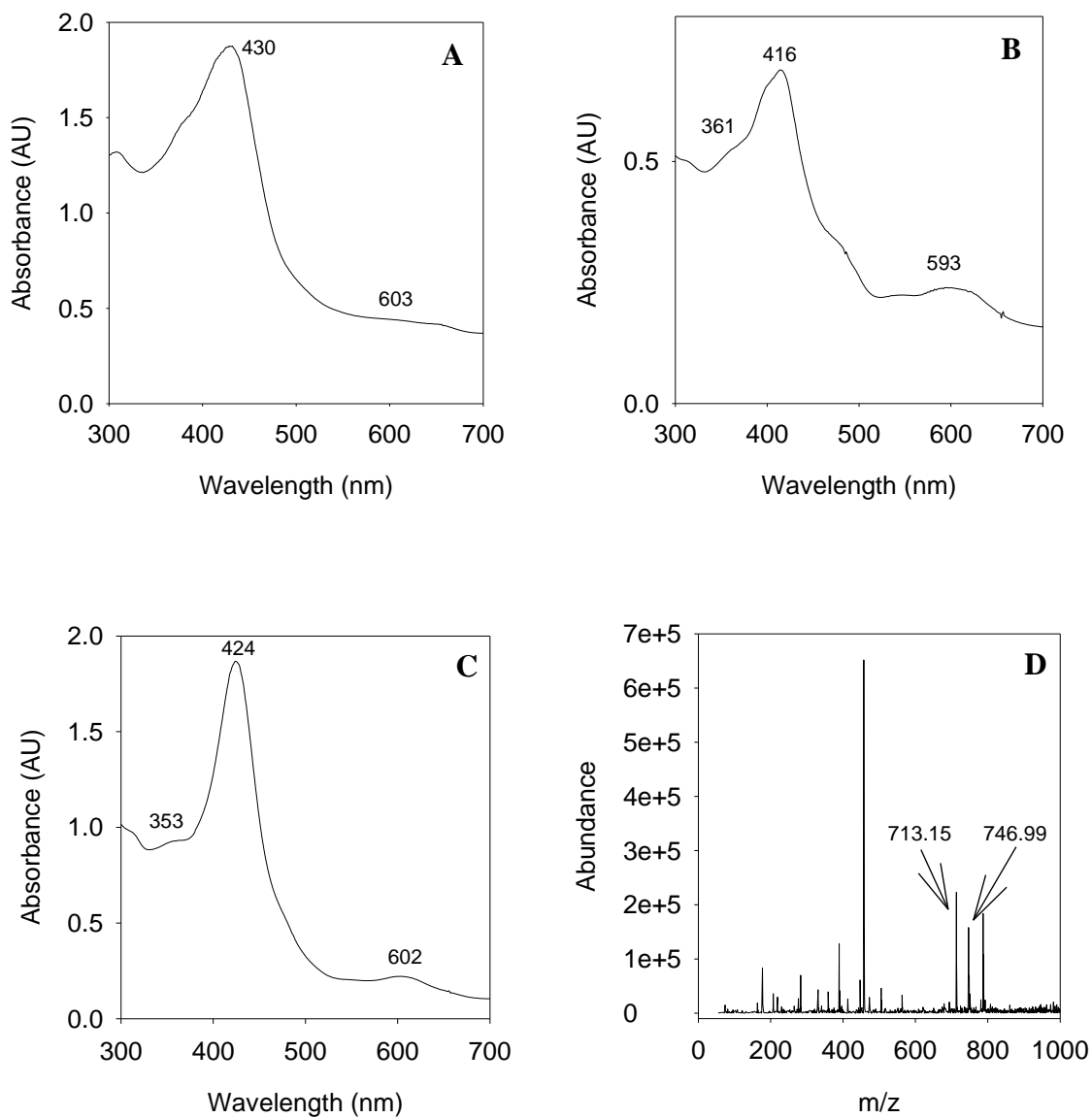


**Figure 2-5.** (A) The UV-vis spectrum of  $[\text{Mn}^{\text{IV}}(\text{TPC})\text{Cl}]$  (**3a**) in  $\text{CH}_2\text{Cl}_2$ ; (B) The UV-vis spectrum of  $[\text{Mn}^{\text{IV}}(\text{TPFC})\text{Cl}]$  (**3b**) in  $\text{CH}_2\text{Cl}_2$ ; (C) The UV-vis spectrum of  $[\text{Mn}^{\text{IV}}(4\text{-NO}_2\text{TPC})\text{Cl}]$  (**3c**) in  $\text{CH}_2\text{Cl}_2$ . (D) ESI-MS spectrum of  $[\text{Mn}^{\text{IV}}(4\text{-NO}_2\text{TPC})\text{Cl}]$  (**3c**).

# CHAPTER 3

## VISIBLE LIGHT-INDUCED FORMATION AND KINETIC STUDIES OF HIGH-VALENT CORROLE-MANGANESE-OXO DERIVATIVES

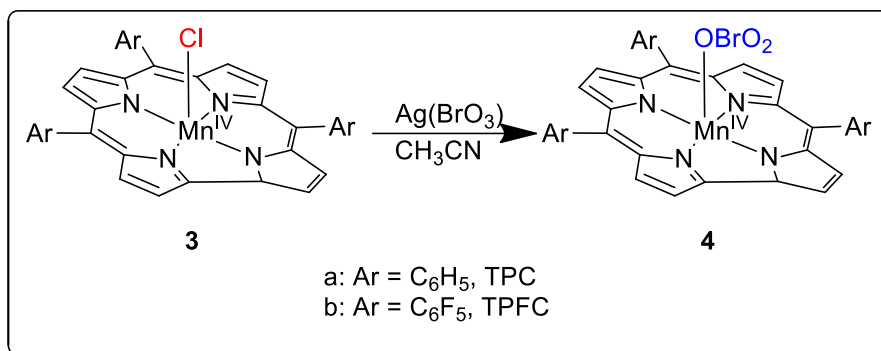
### 3.1 Introduction

Photochemical induced activation of transition metal complexes to yield reactive oxidants has been known for decades.<sup>48</sup> Photochemical production of these reactive metal-oxo species has proven to be much faster when compared to even the fastest mixing chemical reactions. In addition, oxidation kinetics of the photo-generated metal-oxo species produced under single-turnover conditions are not convoluted.<sup>49</sup> As a result, extensive investigations are underway into the formation of high-valent metal-oxo corrole species from photo-induced ligand cleavage reactions with visible light.<sup>50</sup> This advantage allows for the direct kinetic study of their oxygen atom transfer (OAT) reactions with organic substrates. In addition, metal-catalyzed oxidation reactions can be studied and understood using the stable and well-characterized corrole-manganese(V)-oxo species as an important mechanistic probe.<sup>51</sup>

In this chapter, a new photochemical approach to obtaining corrole-manganese(V)-oxo complexes  $[\text{Mn}^{\text{V}}(\text{Cor})\text{O}]$  has been developed. One important factor involving the reactivity of  $[\text{Mn}^{\text{V}}(\text{Cor})\text{O}]$  is to investigate the electronic effect of the oxidizing species. Thus, three manganese(V)-oxo corroles **6** were produced by visible light irradiation of highly photo-labile manganese(IV)-bromate corrole **4** and manganese(IV)-chlorate corrole **5** precursors, respectively. Additionally, spectral and kinetic results demonstrated that the different photo-generated manganese(V)-oxo corroles **6** oxidized substrates through different reaction pathways depending on the nature of the corrole ligands and the solvents.

## 3.2 Results and Discussion

### 3.2.1 Generation of Corrole-Manganese(IV) Bromate Precursors



**Scheme 3-1.** Axial ligand exchange from **3** to **4** with Ag(BrO<sub>3</sub>).

Two manganese(IV) corroles were used for the axial ligand exchange from a chloride ligand to a bromate ligand (Scheme 3-1), each differing in their electron environments. The facile exchange was executed by introducing **3** to an excess amount of Ag(BrO<sub>3</sub>), which was monitored by UV-vis spectroscopy (Fig. 3-1). Species **4** was unable to be isolated for a full spectrophotometric characterization due to their highly photo-labile nature. Therefore, they were immediately used for photochemical reactions following *in situ* formation.

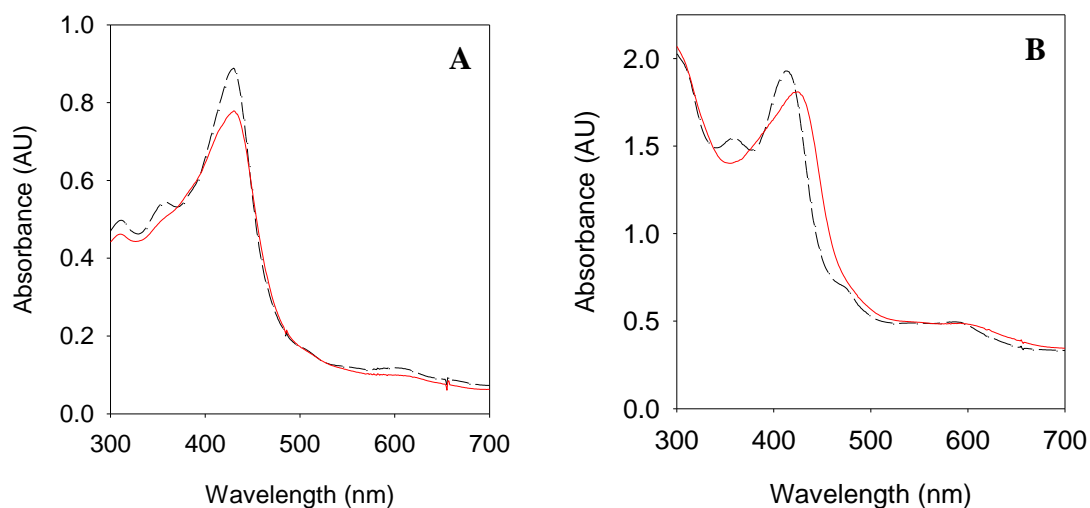
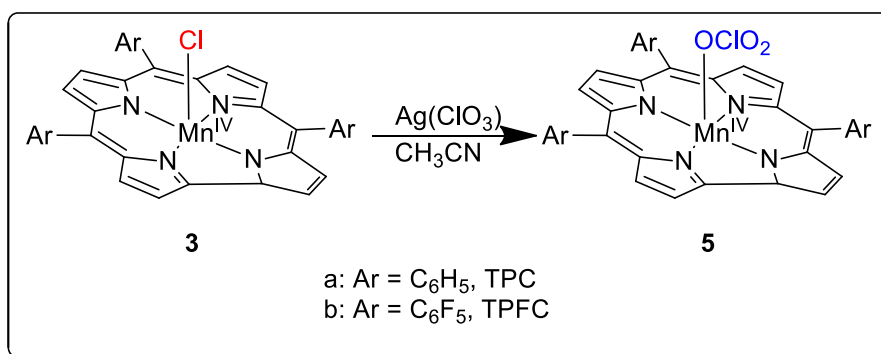


**Figure 3-1.** (A) UV-vis spectra of  $[\text{Mn}^{\text{IV}}(\text{TPC})\text{Cl}]$  (dashed line) and  $[\text{Mn}^{\text{IV}}(\text{TPC})(\text{BrO}_3)]$  (solid line); (B) UV-vis spectra of  $[\text{Mn}^{\text{IV}}(\text{TPFC})\text{Cl}]$  (dashed line) and  $[\text{Mn}^{\text{IV}}(\text{TPFC})(\text{BrO}_3)]$  (solid line).

### 3.2.3 Generation of Corrole-Manganese(IV) Chlorate Precursors

#### $[\text{Mn}^{\text{IV}}(\text{Cor})(\text{ClO}_3)]$



**Scheme 3-2.** Axial ligand exchange from **3** to **5** with  $\text{Ag}(\text{ClO}_3)$ .

Similarly, a second photo-labile species was studied alongside the manganese(IV) bromate species. Manganese(IV) chlorate species were formed via a facile exchange of

the chloride counterion of **3** with excess Ag(ClO<sub>3</sub>). Although Ag(BrO<sub>3</sub>) has proven to be more photoreactive than Ag(ClO<sub>3</sub>), it has a low solubility in CH<sub>3</sub>CN. Ag(ClO<sub>3</sub>), however, is far more soluble in CH<sub>3</sub>CN, making it capable for the facile exchange of the chloride counterion to be completed without being added in extreme excess. This exchange resulted in the corresponding chlorate compounds with the observation of AgCl precipitate. In the same fashion as the bromate species, the chlorate species were also prepared *in situ* and used immediately for photochemical reactions.

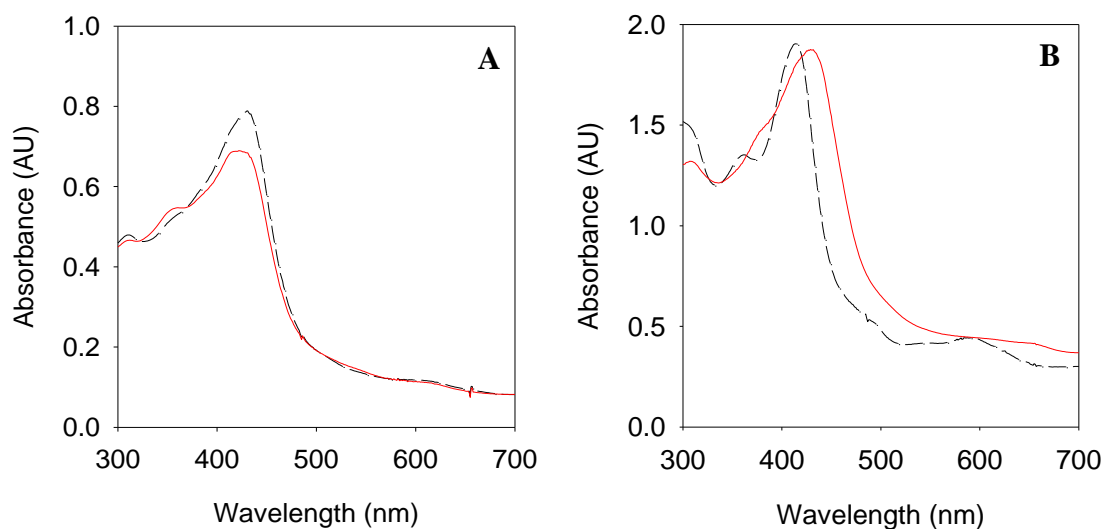
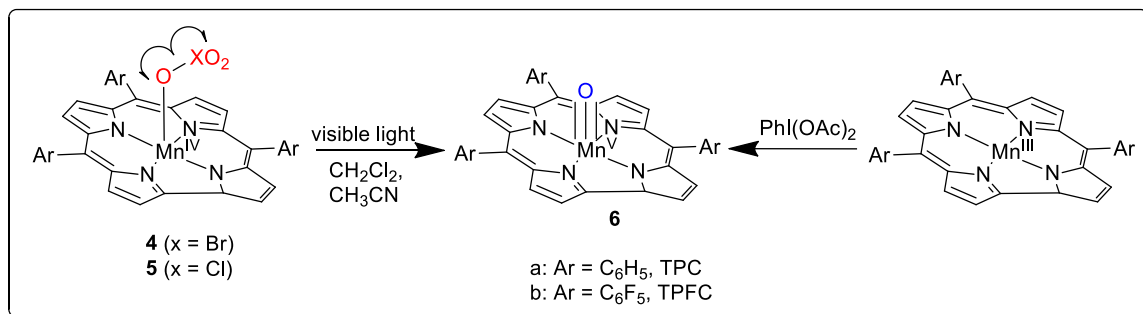


**Figure 3-2.** (A) UV-vis spectra of [Mn<sup>IV</sup>(TPC)Cl] (dashed line) and [Mn<sup>IV</sup>(TPC)(ClO<sub>3</sub>)] (solid line); (B) UV-vis spectra of [Mn<sup>IV</sup>(TPFC)Cl] (dashed line), and [Mn<sup>IV</sup>(TPFC)(ClO<sub>3</sub>)] (solid line).

### 3.2.4 Visible Light Generation of Manganese(V)-Oxo Corroles



**Scheme 3-3.** Photochemical and chemical formation of manganese(V)-oxo corroles **6**.

Generation of corrole-manganese(V)-oxo species **6** from complexes **4a** and **4b** were conducted in anaerobic CH<sub>3</sub>CN with visible light from a SOLA engine (60W). This resulted in changes in the absorption spectra showing formation of **6** indicated by a blue shift in the Soret band. The non-electron-deficient **6a** spectrum was similar to that of **6b**, however, exhibited a far weaker blue-shifted Soret band and was instead shown as a shoulder (Fig. 3-3 A). The formation of the electron-deficient **6b** was far more evident, as shown in Fig. 3-3 B by the growth in the Soret peak at 346 nm. Species **6b** displayed split Soret bands that are distinct with a strong blue-shifted band. It is important to note that the formation of both **6a** and **6b** via visible light generation matched the spectra for their formation from previous chemical oxidations of the corresponding manganese(III) precursors with ozone or PhIO.<sup>47,52</sup> Based on the electrophilic nature of the corrole-manganese(V)-oxo species, it is expected that the TPC complex (**6a**) will be more stable (less reactive) than the TPFC complex (**6b**).

Photochemical oxidative formation of **6a** was observed to be faster than that of the formation for **6b**. Aryl groups on the TPC system are less electron-withdrawing than in the

case of TPF systems. In view of lower oxidation potentials of TPC systems, the thermodynamically favored **4a** undergoes photo-oxidation more readily to form **6a**.

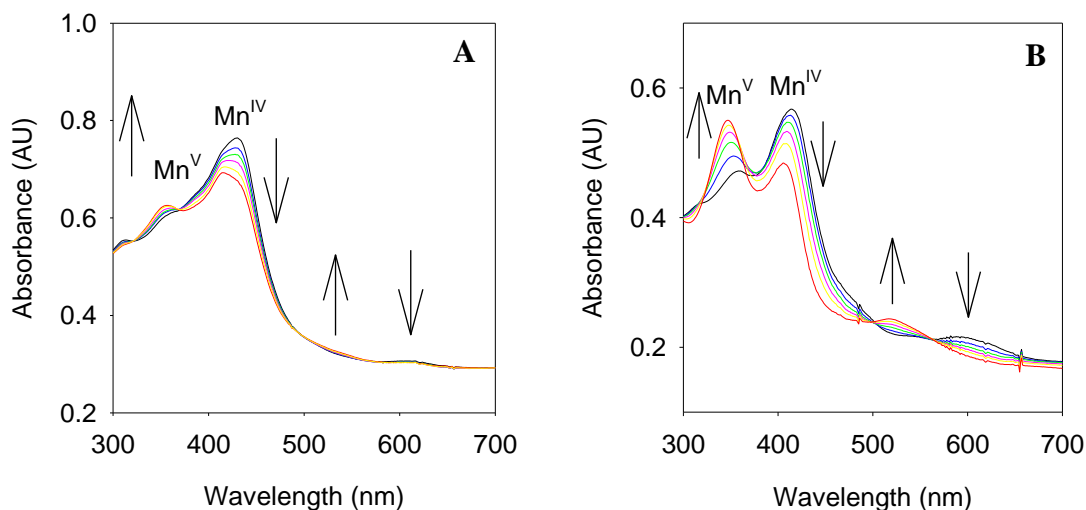


**Figure 3-3.** (A) Time resolved formation spectra of **6a** (red line) following visible light irradiation of **4a** ( $8.0 \times 10^{-6}$  M) over 30 s in anaerobic CH<sub>3</sub>CN solution at 23 °C. (B) Time resolved formation spectra of **6b** (red line) following visible light irradiation of **4b** ( $7.0 \times 10^{-6}$ ) over 80 s in anaerobic CH<sub>3</sub>CN solution at 23 °C.

In addition to the bromate precursors, chlorate precursors (**5**) were also generated and oxidatively converted to **6**. Formation of **6a** from **5a** (Fig. 3-4 A) and of **6b** from **5b** (Fig. 3-4 B) were monitored via time-resolved UV-vis spectra.

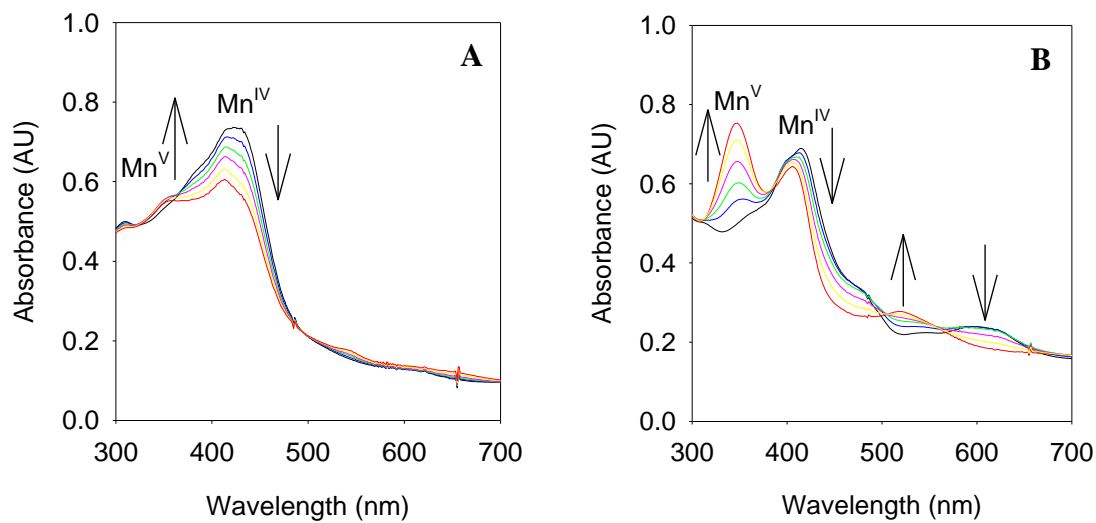


**Figure 3-4.** (A) Time resolved formation spectra of **6a** (red line) following visible light irradiation of **5a** ( $8.0 \times 10^{-6}$ ) over 200 s in anaerobic  $\text{CH}_3\text{CN}$  solution at 23 °C. (B) Time resolved formation spectra of **6b** (red line) following visible light irradiation of **5b** ( $8.0 \times 10^{-6}$  M) over 300 s in anaerobic  $\text{CH}_3\text{CN}$  solution at 23 °C.

Visible light irradiation of bromate (**4**) and chlorate (**5**) precursors to form corrole manganese(V)-oxo species, **6**, is attributed to the homolytic cleavage of the O-Br and O-Cl bonds which results in a one-electron photo-oxidation. We found that the photochemical cleavage of the bromate species was far more efficient and faster than that of the chlorate ligands. Control experiments were conducted and showed that species **6** was not formed in the absence of light. As expected, using a more intense light source (SOLA, 120 W) significantly decreased the time of formation of **6b**. However, photo-degradation was observed for **6a** when using the more intense light.

Prior to testing for the visible-light generation of **6**, **3a** and **3b** were chemically oxidized with  $\text{PhI}(\text{OAc})_2$  to provide a standard for the formation of **6**. The representative formation of **6b** from **3b** is shown below in Fig. 3-5. The characteristic UV-vis spectra obtained from the photochemical generation of **6a** and **6b** were matching those from previously reported chemical oxidation methods.<sup>47,52</sup>

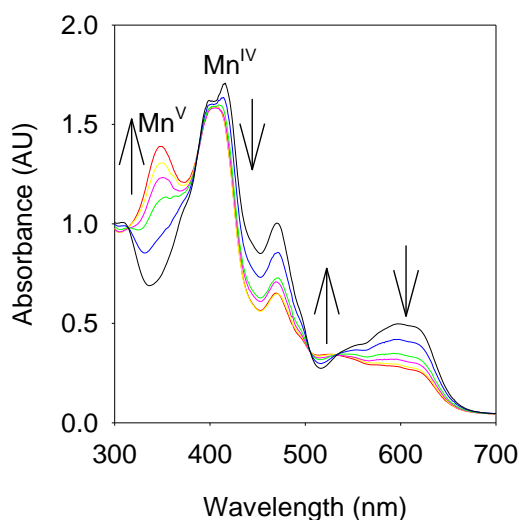


**Figure 3-5.** Chemical formation of **6b** from reaction between  $[\text{Mn}^{\text{IV}}(\text{TPFC})\text{Cl}]$  (**3b**) and  $\text{PhI}(\text{OAc})_2$  (2 equiv.) in  $\text{CH}_3\text{CN}$  over 40 s.

### 3.2.5 Kinetic Studies of High-Valent Corrole-Manganese-Oxo Species

Following the formation of species **6**, oxidation reaction kinetics experiments were conducted with alkanes, activated hydrocarbon, and thioanisoles at similar concentrations of approximately  $5.0 \times 10^{-6}$  M in both  $\text{CH}_2\text{Cl}_2$  and  $\text{CH}_3\text{CN}$ . Earlier reports demonstrated a dependency on catalyst concentration for oxidation reactions.<sup>25</sup> For kinetic studies, the pseudo-first-order rate constants were measured spectroscopically following the addition

of excess amount of substrate to the manganese(V)-oxo species that was formed *in situ*. For species **6a** it was observed that the Mn<sup>IV</sup> was regenerated in both solvents, identified by the transition of the Soret peak from the  $\lambda_{\text{max}}$  for Mn<sup>V</sup> species at 348 nm to the known  $\lambda_{\text{max}}$  for Mn<sup>IV</sup> species at 430 nm (Fig. 3-6). This transformation does not implicate a one-electron oxidation reaction from Mn<sup>V</sup>(O) to Mn<sup>IV</sup> species in view of the relatively slow reaction rate.

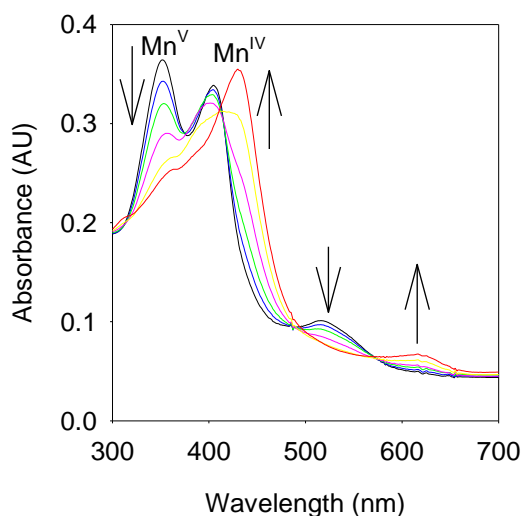


**Figure 3-6.** Time-resolved spectra of **6a** in CH<sub>3</sub>CN reacting with thioanisole (6 mM) over 40 s.

In contrast, with the more electron-deficient system **6b** the Soret band decayed to two different products depending on the choice of solvent. In CH<sub>3</sub>CN, **6b** regenerates a Mn<sup>III</sup> species characterized by its known  $\lambda_{\text{max}}$  at 465 nm (Fig. 3-7 A). This reaction sequence is consistent with a direct two-electron oxidation from Mn<sup>V</sup> to Mn<sup>III</sup>. In CH<sub>2</sub>Cl<sub>2</sub>, the Mn<sup>IV</sup> species is regenerated from **6b** (Fig. 3-7 B), as it was with the **6a** species. This

solvent effect can be attributed to a variety or combination of effects including but not limited to polarity differences and electron environment effects.

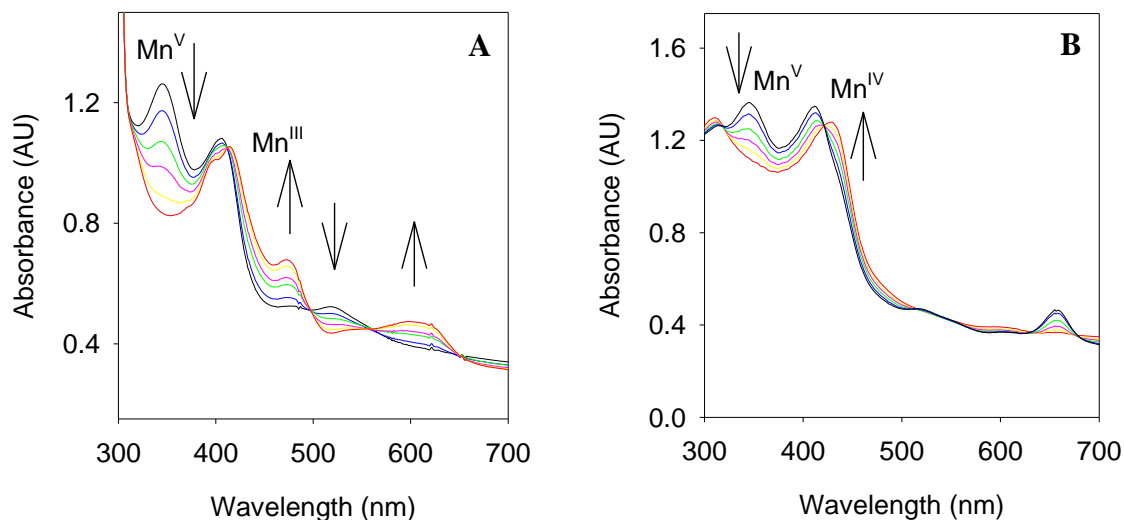


**Figure 3-7.** (A) Time-resolved spectra of **6b** in CH<sub>3</sub>CN reacting with cyclohexene (0.5 M) over 1000 s. (B) Time-resolved spectra of **6b** in CH<sub>2</sub>Cl<sub>2</sub> with cyclohexene (0.5 M) over 300 s.

Substrate concentrations were varied allowing for the comparison of each pseudo-first-order decay rate constant ( $k_{\text{obs}}$ ) for **6** resulting in a linear increase with substrate concentrations (Fig. 3-8 A). Apparent second-order rate constants ( $k_{\text{ox}}$ ) for various substrates (Table 3-1) were calculated. Table 3-1 shows the trends in the  $k_{\text{ox}}$  for the various substrates; i.e. organic sulfides are approximately 3 to 4 orders of magnitude more reactive when comparing them to alkanes or ethylbenzene for the same oxo corrole.

**Table 3-1.** Second-order rate constants for reactions with various substrates.<sup>a</sup>

Oxo species	Substrates	$k_{ox}(M^{-1}s^{-1})$	
		CH <sub>3</sub> CN	CH <sub>2</sub> Cl <sub>2</sub>
<b>6a</b>	Cyclohexene	$(10.0 \pm 1.0) \times 10^{-2}$	
	<i>Cis</i> -Cyclooctene	$(5.0 \pm 0.6) \times 10^{-2}$	
	PhEt	$(2.1 \pm 0.3) \times 10^{-3}$	
	PhSMe	6.0 ± 0.8	
	<i>p</i> -MeO-PhSMe	85.5 ± 2.4	
	<i>p</i> -F-PhSMe	24.8 ± 1.5	
	<i>p</i> -Cl-PhSMe	5.3 ± 0.3	
<b>6b</b>	Cyclohexene	$(3.4 \pm 0.2) \times 10^{-3}$	$(1.6 \pm 0.2) \times 10^{-2}$
	Cyclohexene <sup>b</sup>	$(3.9 \pm 0.4) \times 10^{-3}$	$(1.5 \pm 0.1) \times 10^{-2}$
	<i>cis</i> -Cyclooctene	$(2.9 \pm 0.2) \times 10^{-3}$	$(0.1 \pm 0.1) \times 10^{-2}$
	PhEt	$(1.4 \pm 0.1) \times 10^{-4}$	$(2.7 \pm 0.3) \times 10^{-4}$
	Styrene	$(3.0 \pm 0.1) \times 10^{-3}$	
	PhSMe	4.9 ± 0.4	
	<i>p</i> -MeO-PhSMe	62.0 ± 0.7	
	<i>p</i> -Me-PhSMe	22.0 ± 0.6	
	<i>p</i> -F-PhSMe	6.7 ± 0.5	
	<i>p</i> -Cl-PhSMe	3.6 ± 0.3	

<sup>a</sup> For both CH<sub>3</sub>CN and CH<sub>2</sub>Cl<sub>2</sub>, the values collected were at average of three runs with 2σ standard deviation at 2.0 × 10<sup>-5</sup> M concentration at 23 ± 2 °C.

<sup>b</sup> From **6b** generated by chemical oxidation of **2a**.<sup>52</sup>

In regards to the *para*-substituted thioanisoles (X-thioanisoles; X = 4-MeO, 4-Me, 4-F, and 4-Cl), a significant substituent dependency was observed for the second-order rate constants, for reaction with **6b**, as shown by the linear correlation (R = 0.99) of the Hammett plot below in Fig. 3-8 B. It was observed that the more electron-withdrawing *para*-substituted functional groups resulted in slower reactions. Thus, the plotting of  $\log(k_{\text{rel}})$ , where  $k_{\text{rel}}$  was solved according to

$$k_{\text{rel}} = k(\textit{para}\text{-X-thioanisole})/k(\text{thioanisole}) \quad \text{Eq. 2,}$$

versus the corresponding Hammett  $\sigma^+$  substituent constant<sup>53</sup> resulted in a slope of  $-1.34 \pm 0.18$ .

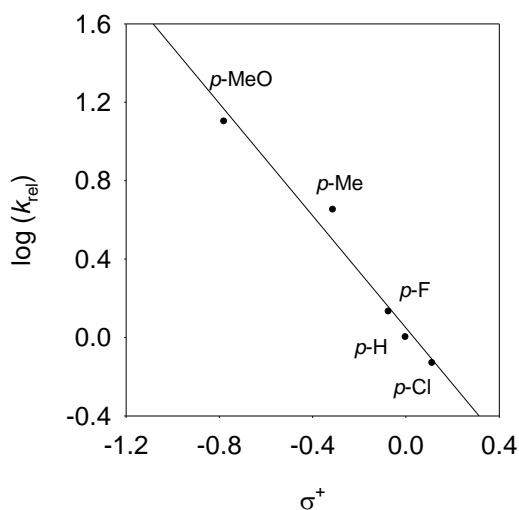


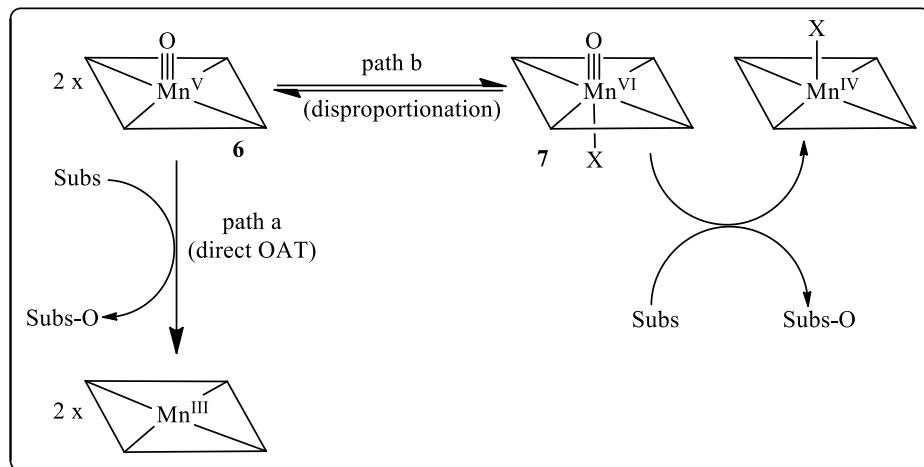
**Figure 3-8.** (A) Kinetic plots of the observed rate constants ( $k_{\text{obs}}$ ) of **6b** versus the concentration of various *para*-substituted thioanisoles. (B) Hammett plot for oxidations of *para*-substituted thioanisoles with **6b** in  $\text{CH}_3\text{CN}$ .

Results in Table 3-1 show that there is an inverted reactivity pattern from expected, for the two systems studied, due to the reactions of **6a** being faster with any given substrate than the more electron withdrawing **6b** system. These kinetic results support previously proposed mechanistic models for the disproportionation of **6** to give Mn<sup>IV</sup> corrole and a manganese(VI)-oxo corrole species as the predominant oxidant in these systems.<sup>33,47,25</sup>

### 3.2.6 A Proposed Mechanism

Photo-labile manganese(IV)-corrole species, i.e. [Mn<sup>IV</sup>(Cor)(BrO<sub>3</sub>)] and [Mn<sup>IV</sup>(Cor)(ClO<sub>3</sub>)], were found to form manganese(V)-oxo corrole species via visible light irradiation. This photochemical reaction is due to the homolytic cleavage of the photo labile ligands, resulting in a one-electron oxidation to generate manganese(V)-oxo species.

Kinetic results support the mechanistic model for disproportionation of **6** to give the higher-valent [Mn<sup>VI</sup>(Cor)O] **7** as a more reactive cationic species that functions as the dominant oxidant.<sup>33,47,25</sup> In practice, the lack of observation of **7** spectroscopically is due to its low concentration in solution and its high reactivity. If **7** is the true oxidant, it should be noted that the disproportionation reaction for the formation of species **7** should be more favorable for ligands that have less electron-demand; i.e. that the TPC system would be more favorable than TPFC ligands. Thus, the observed kinetics for the formation of **7** would be controlled by the equilibrium constant of disproportionation, which should be larger for the TPC ligand.<sup>25</sup> When used for the oxidation of organic substrates, we propose that oxidation with [Mn<sup>V</sup>(Cor)(O)] species may undergo two different pathways (Scheme 3-4) based on observations of the decay spectra and kinetic studies.



**Scheme 3-4.** Two oxidation pathways for corrole-manganese(V)-oxo species, **6** controlled by the nature of the ligands and solvents.

The oxidation pathways were dependent on both the electron nature of the corrole ligand as well as a solvent effect. In the case of TPC, paired with the polar  $\text{CH}_3\text{CN}$  or less polar  $\text{CH}_2\text{Cl}_2$  solvents, the disproportionation reaction is favored to form  $\text{Mn}^{\text{VI}}$ -oxo **7** from **6** as the active oxidant for oxidation (path b). Photo-disproportionation of **6a** results in the formation of highly reactive **7a** along with one molecule of a  $\text{Mn}^{\text{IV}}$  product; furthermore, oxidation of an organic reductant by **7a** yields a second molecule of  $\text{Mn}^{\text{IV}}$  product. The proposed  $\text{Mn}^{\text{VI}}$ -oxo compound does not accumulate due to the rate of its reactivity being much greater than the rate of its formation. In contrast, the more electron-deficient corrole system of TPFC in  $\text{CH}_3\text{CN}$  will result in a direct OAT reaction (path a) as the dominant pathway; thus, forming  $\text{Mn}^{\text{III}}$  products following oxidation by  $\text{Mn}^{\text{V}}$ -oxo species. However, when in solution of  $\text{CH}_2\text{Cl}_2$ , the pathway of direct OAT becomes less favorable for the TPFC system. The resulting decay is to  $\text{Mn}^{\text{IV}}$  species due to the disproportionation reaction gaining dominance.

# CHAPTER 4

## OXIDATION OF ORGANIC SULFIDES CATALYZED BY CORROLE-MANGANESE COMPLEXES WITH IODOBENZENE DIACETATE

### 4.1 Introduction

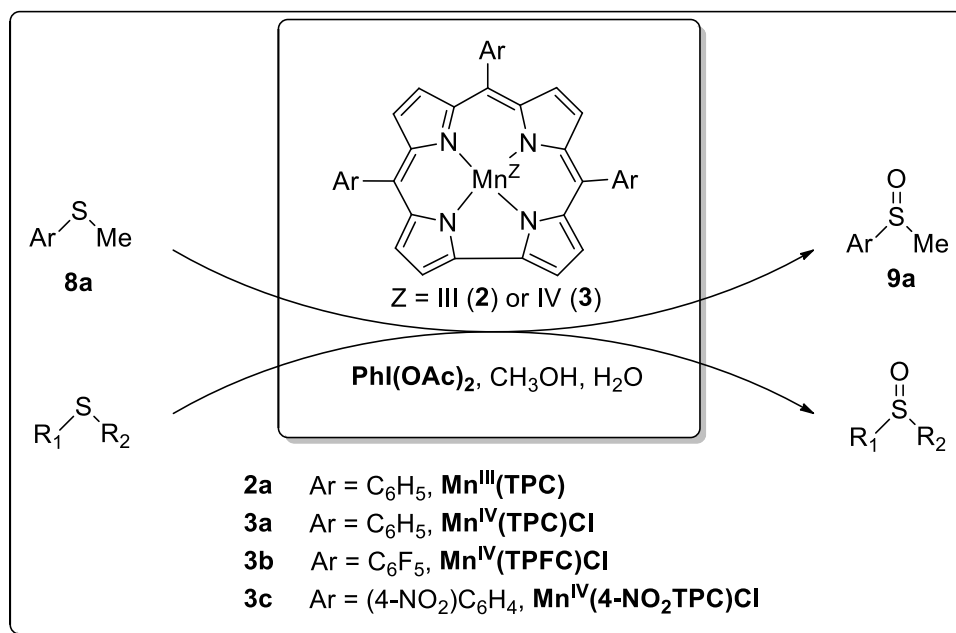
Organic sulfoxides are of great significance as valuable synthetic intermediates in biological systems for production of natural products and significant biological molecules. Thus, the selective oxidation of organic sulfides to sulfoxides is very important.<sup>54</sup> To date, in almost all reported catalytic sulfoxidations, H<sub>2</sub>O<sub>2</sub> is the most commonly used oxygen source for it being inexpensive, ecofriendly, and readily available.<sup>54,55</sup> With H<sub>2</sub>O<sub>2</sub>, various catalysts have been used for catalytic sulfoxidation reactions. However, many of them lead to the unwanted over-oxidation to sulfones and most procedures rarely provide an ideal combination of high selectivity for sulfoxide formation, quick reactions, and high yields.

Metallocorroles have been used for a wide variety of catalytic oxidation reactions.<sup>56-58</sup> The first reported example was conducted by Gross and coworkers in 1999 by using iron(IV) *tris*(pentafluorophenyl)corrole [Fe<sup>IV</sup>(TPFC)] with the sacrificial oxidant iodosobenzene (PhIO).<sup>59</sup> Later, the same group conducted similar biomimetic oxidations with Mn<sup>III</sup>(TPFC).<sup>15</sup> Nonetheless, the use of metallocorroles has proven to show limited success with poor selectivity and low efficiency.

One problem associated with metallocorrole catalysts is that most metallocorroles are prone to oxidative degradation. Commonly used sacrificial oxygen sources such as *m*CPBA and PhIO are too strong and can lead to catalyst degradation. In contrast, the less commonly used iodobenzene diacetate [PhI(OAc)<sub>2</sub>] does not damage the metal catalysts

nor show appreciable reactivity to the sulfide substrate under normal catalytic conditions. Recently, in two separate studies, it was revealed that an efficient oxidation of alkanes via  $\text{PhI}(\text{OAc})_2$  catalyzed by electron deficient iron(III) corroles<sup>60</sup> as well as a study involving  $\text{PhI}(\text{OAc})_2$  as an oxidant for the efficient and chemoselective oxidation of sulfides with iron corrole catalyst.<sup>61</sup>

In an attempt to further explore the use of  $\text{PhI}(\text{OAc})_2$  for the efficient and chemoselective oxidation of sulfides to sulfoxides, a new protocol for catalytic sulfoxidations with manganese corrole systems as the metal catalyst using  $\text{PhI}(\text{OAc})_2$  as the sacrificial oxidant has been developed. In most cases, various substituted thioanisoles and sulfide compounds were successfully oxidized to their corresponding sulfoxides with excellent chemoselectivity and quantitative conversions (Scheme 4-1).



**Scheme 4-1.** Catalytic sulfoxidations by a variety of corrole-manganese catalysts in the presence of  $\text{PhI}(\text{OAc})_2$  and water.

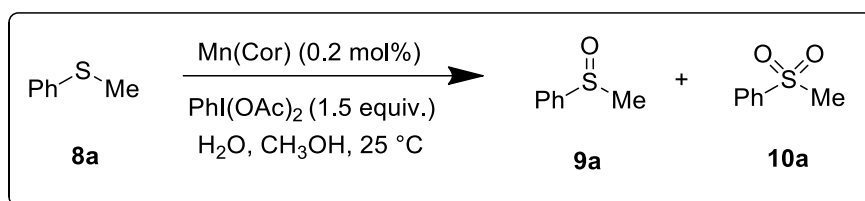
## 4.2 Results and Discussion

### 4.2.1 Screening Studies in the Catalytic Oxidation of Thioanisole

Although  $\text{PhI}(\text{OAc})_2$  has been used as a mild oxidizing agent previously, it has not been tested for manganese corrole-catalyzed sulfoxidation reactions. Therefore,  $\text{PhI}(\text{OAc})_2$  was first used with manganese corroles (**2** and **3**) with varying electronic environments to evaluate the catalytic oxidation of thioanisole (**8a**). At room temperature, catalytic reactions were performed in methanol with a 1:1.5 ratio of thioanisole (0.5 mmol) to  $\text{PhI}(\text{OAc})_2$  (0.75 mmol), catalyst (1  $\mu\text{mol}$ ), and water (4.5  $\mu\text{L}$ ) were added to the reaction solution. Although the data are not shown here, these optimal conditions were found through multiple trials including solvent effect testing, where  $\text{CH}_3\text{OH}$  was found to allow for faster reactions than  $\text{CH}_3\text{CN}$  and  $\text{CHCl}_3$ . Previously, studies on iron(III)porphyrin/corrole-catalyzed epoxidations<sup>50,60</sup> and iron(III)corrole-catalyzed sulfoxidations<sup>61</sup> reported that a small amount of water, along with the  $\text{PhI}(\text{OAc})_2$  oxidant, resulted in accelerating the catalytic effects in the porphyrin and corrole systems. Presumably, the water gradually induces the formation of  $\text{PhIO}$ , a stronger oxidant, from  $\text{PhI}(\text{OAc})_2$ .<sup>50</sup> Furthermore, addition of water allows for the production of stable  $\text{HOAc}$  instead of anhydride  $\text{Ac}_2\text{O}$  under anhydrous conditions. It was extremely apparent through screening studies that the same water effects were consistent across all catalysts used for this study. As reported previously, methyl phenyl sulfoxide (**9a**) was produced as the only product by iron(III) corrole catalysts with only 4.5  $\mu\text{L}$  of water. The addition of more water resulted in a faster reaction but a lower chemoselectivity, i.e., over-oxidation to methyl phenyl sulfone (**10a**) was found. The four manganese corroles used for catalytic oxidations in this study were all tested in  $\text{CH}_3\text{OH}$  (2 mL) with only 4.5  $\mu\text{L}$  of water in conjuncture

with the previous studies. The percent conversions and selectivity's for each catalyst, depicted in Table 4-1, were analyzed by either GC-MS or <sup>1</sup>H-NMR and calculated based on the ratios of peak area of the substrate and oxidized products.

**Table 4-1.** Catalytic oxidation of thioanisole by 2 and 3 with PhI(OAc)<sub>2</sub>.<sup>a</sup>



Entry	Catalyst	Time (h)	Conversion (%) <sup>b</sup>	Selectivity ( <b>9:10</b> ) <sup>b</sup>
1	<b>2a</b> Mn <sup>III</sup> (TPC)	1.3	> 99	95:05
2	<b>3a</b> Mn <sup>IV</sup> (TPC)Cl	1	> 99	97:03
3	<b>3b</b> Mn <sup>IV</sup> (TPFC)Cl	1	85	90:10
4	<b>3c</b> Mn <sup>IV</sup> (4-NO <sub>2</sub> TPC)Cl	1.5	> 99	94:06

<sup>a</sup> All reactions were performed in CH<sub>3</sub>OH (2 mL) with a 1:1.5 molar ratio of substrate to oxidant and 0.2 mol% catalyst with a substrate concentration of 0.25 M.

<sup>b</sup> Conversion percentages and selectivity were determined by <sup>1</sup>H-NMR and quantitative GC-MS analysis on the crude reaction mixture diluted in CH<sub>3</sub>OH.

Fig. 4-1 shows the reaction profiles for the catalytic sulfoxidation reactions of **8a** based on the data depicted in Table 4-1. It is observed that there is an effect by the corrole ligands and oxidation states of the manganese metal. In general, Mn<sup>IV</sup> catalysts showed faster reactions than Mn<sup>III</sup> catalysts (Table 4-1, entries 1 and 2). This indicates that Mn<sup>IV</sup>

catalysts have a faster access to generate the oxidizing metal-oxo intermediates than the  $\text{Mn}^{\text{III}}$  catalysts with the same oxygen source.

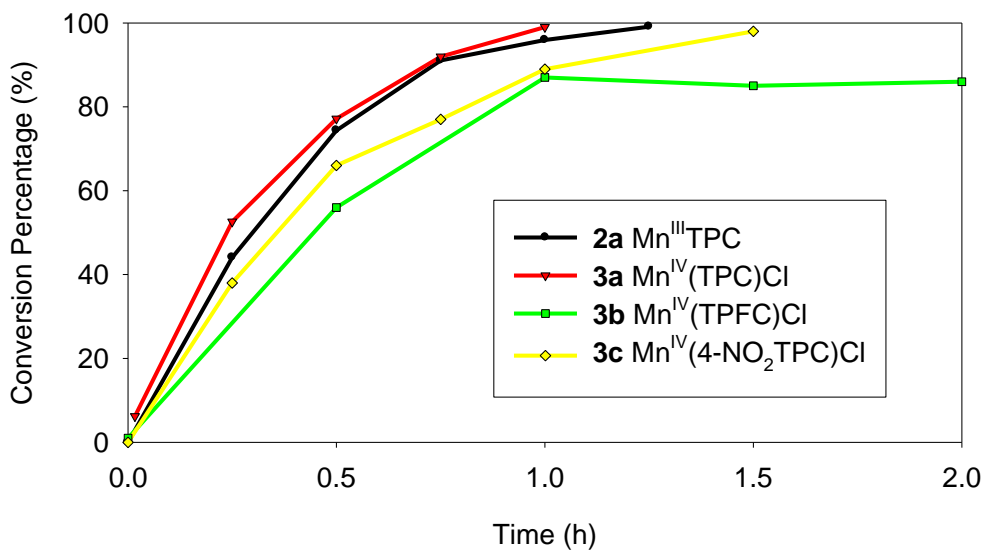
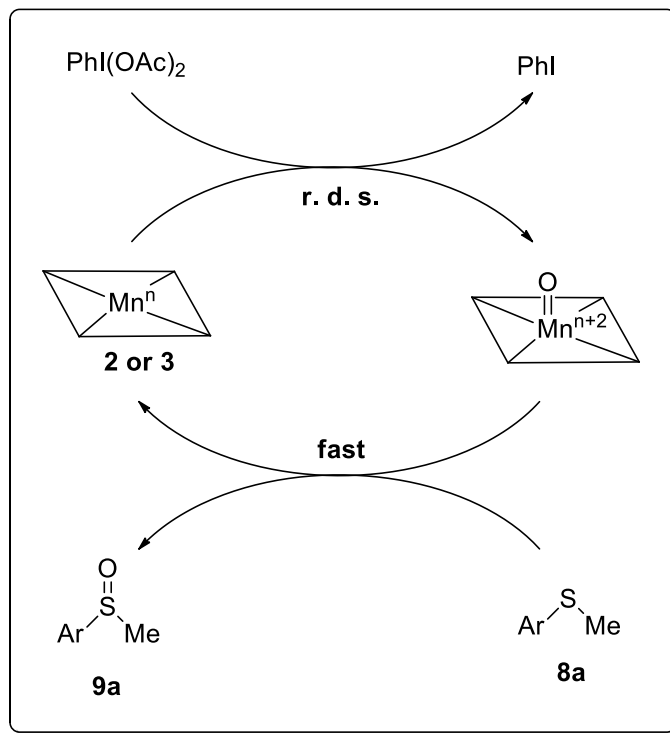


**Figure 4-1.** Reaction profiles for the catalytic oxidation of thioanisole with various catalyst.

Furthermore, when comparing results between different catalysts of the same oxidation state (Table 4-1, entries 2-4), the catalysts with more electron-withdrawing corrole ligands led to a slower rate of reaction. This observation suggests that the formation of the metal-oxo intermediate from the catalyst reacting with  $\text{PhI}(\text{OAc})_2$  is the rate-determining step during the catalytic process. The oxygen transfer from the metal-oxo species to the organic substrate is the faster step as proposed in Scheme 4-2.

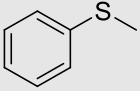
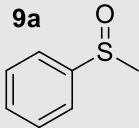
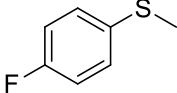
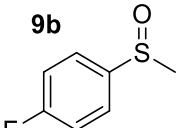
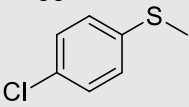
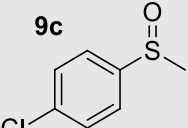
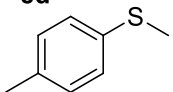
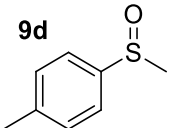
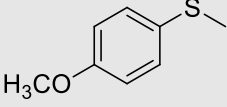
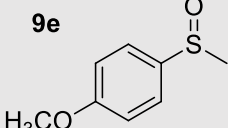
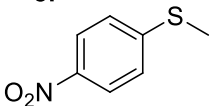
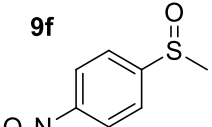
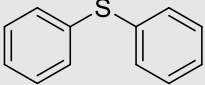
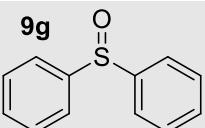
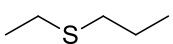
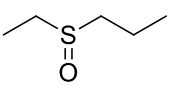
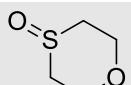


**Scheme 4-2.** Proposed mechanism for catalytic sulfoxidation by manganese corroles with  $\text{PhI}(\text{OAc})_2$ .

#### 4.2.2 Substrate Scope

Under optimal conditions, the substrate scope for catalytic oxidations of other substrates were further explored. In total, ten substrates were tested: thioanisole (**8a**), 4-chlorothioanisole (**8b**), 4-fluorothioanisole (**8c**), 4-methylthioanisole (**8d**), 4-methoxythioanisole (**8e**), 4-nitrothioanisole (**8f**), diphenyl sulfide (**8g**), ethyl propyl sulfide (**8h**), and 1,4-oxathiane (**8i**). Each reaction was monitored by  $^1\text{H-NMR}$  and/or GC-MS at various time intervals to determine the percent conversion of substrate to product as well as the selectivity ratio of sulfoxide (**9**) to sulfone (**10**). Table 4-2 lists the expected product **9** with their corresponding selectivity for the corrole-catalyzed sulfoxidation reactions using **3a** as the catalyst. As evident in Table 4-2, high selectivities of sulfoxides over

**Table 4-2.** Corrole-catalyzed sulfoxidation for sulfide substrates by 3a.

Entry	Substrate	Time (h)	Conv. % <sup>b</sup>	Product	Selectivity (9:10) <sup>b</sup>
1	<b>8a</b> 	1	99	<b>9a</b> 	97:03
2	<b>8b</b> 	2	88	<b>9b</b> 	99:01
3	<b>8c</b> 	2	76	<b>9c</b> 	98:02
4	<b>8d</b> 	1	95	<b>9d</b> 	97:03
5	<b>8e</b> 	1	99	<b>9e</b> 	99:01
6	<b>8f</b> 	6	93	<b>9f</b> 	99:01
7	<b>8g</b> 	4	95	<b>9g</b> 	95:05
8	<b>8h</b> 	1	76	<b>9h</b> 	99:01
9	<b>8i</b> 	1	99	<b>9i</b> 	99:01

<sup>a</sup> Unless otherwise specified, all reactions were performed in CH<sub>3</sub>OH (2 mL), with PhI(OAc)<sub>2</sub> (0.75 mmol), substrate (0.5 mmol), [Mn<sup>IV</sup>(TPC)Cl], and H<sub>2</sub>O (4.5 μL).

<sup>b</sup> Based on the conversion from substrate to products. Analyzed by <sup>1</sup>H-NMR and/or GC-MS analysis of crude products in CH<sub>3</sub>OH.

sulfones and good to quantitative conversions are observed in most cases. The relationship between time and conversion percentage is relevant because it indicates the selective and efficient nature of the catalyst. It is important to note that in reactions for **8f** there was obvious catalyst degradation, which resulted in a slower reaction due to the bleaching of the catalyst (entry 6).

The reaction profiles were plotted as the percent substrate conversion vs. time as shown in Fig. 4-2. Based on the reaction profiles, a reactivity trend was observed in terms of the electronic environments of the substrates used in this study. Generally, sulfides substrates with more electron-withdrawing substituents led to slower reactions. This was extremely apparent in the reactions of various *para*-substituted thioanisoles. For example, 4-methoxythioanisole (**8e**) resulted in a much faster reaction than the thioanisole substrate (**8a**). On the contrary, 4-nitrothioanisole (**8f**) resulted in the slowest reaction. This can be explained by the reduced nucleophilicity of sulfide due to the electron-withdrawing substituents on the substrate. Although the substrates consistently followed this trend, one compound differed. Diphenyl sulfide, **8g**, should have allowed for the reaction to proceed faster than **8a**. However, sulfoxidation of **8g** took four times as long as it did for **8a**. This can be explained due to the steric effect of two bulky phenyl groups making **8g** harder to access the oxidizing intermediate for the oxo transfer reaction.

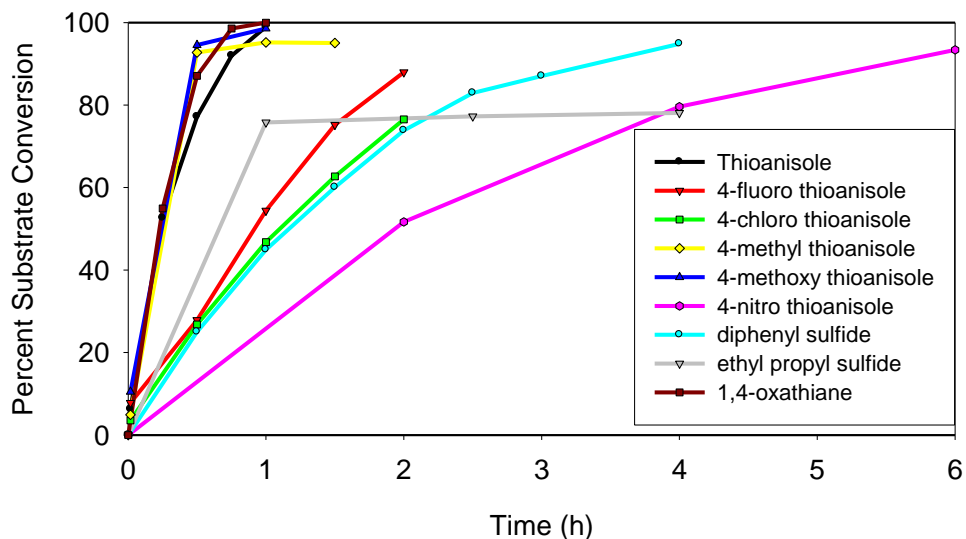


**Figure 4-2.** Reaction profiles for the sulfoxidation of various para-substituted thioanisoles and sulfide substrates with 3a as the catalyst.

### 4.2.3 Competition Studies

Competition studies were performed in order to assess whether the high-valent manganese(V)-oxo species is the active oxidant under catalytic oxidation conditions. As previously reported, **2** can be oxidized to form a manganese(V)-oxo species that then decays to a manganese(IV) species.<sup>61</sup> However, the observation of the manganese(V)-oxo species does not necessarily suggest it is the active oxidant under catalytic turnover conditions. By comparing the ratios of products formed under catalytic turnover conditions to the ratios of rate constants measured in direct kinetic studies, one can evaluate whether the same species is active under both sets of conditions. If the same oxidant is present in both cases, the relative rate constants from competitive studies would be similar to the ratios of absolute rate constants obtained from direct measurements. If the ratios were not

similar, it can be concluded that the active oxidant is different under the differing conditions. Toward this end, the competitive sulfoxidation reactions catalyzed by manganese corrole species **3a** with PhI(OAc)<sub>2</sub> as the sacrificial oxygen source were conducted as described in the experimental section. Table 4-3 contains the results from previously reported kinetic studies<sup>61</sup> and catalytic competition results for two *para*-substituted thioanisole substrates, **8b** and **8e**. These two were chosen because they represented different electron environments of substrates.

**Table 4-3.** Relative rate constants from kinetic studies and competitive catalytic studies.<sup>a</sup>

Entry	Catalyst	Substrates	Method	$k_{rel}^b$
1	Mn <sup>IV</sup> (TPC)Cl <b>3a</b>	<i>p</i> -F-PhSMe/PhSMe	Kinetic results <sup>c</sup>	4.13
2			PhI(OAc) <sub>2</sub>	0.62
3		<i>p</i> -MeO-PhSMe/PhSMe	Kinetic results <sup>c</sup>	14.25
4			PhI(OAc) <sub>2</sub>	4.55

<sup>a</sup> Equal amounts of two substrates, e.g. thioanisole (0.25 mmol) and substituted thioanisole (0.25 mmol), **3a** catalyst (1 μmol), H<sub>2</sub>O (4.5 μL), and PhI(OAc)<sub>2</sub> (0.1 mmol) in CH<sub>3</sub>OH (2 mL) was stirred for ca. 20 to 30 min at 23 ± 2 °C.

<sup>b</sup> Relative ratios of absolute rate constants from kinetic results and competitive oxidations with **3a** at ambient temperature.

<sup>c</sup> Kinetic results were calculated based on data collected from previously reported data.<sup>61</sup>

In this study,  $\text{PhI}(\text{OAc})_2$  was added in a limiting amount to control the conversion to be  $< 20\%$ . GC-MS was used to determine the amounts of oxidation products that were formed. Each sulfide substrate was oxidized in nearly quantitative yields based on the consumption of the oxidant and without the formation of the corresponding over-oxidation product sulfone. As evident in Table 4-3, the ratios of absolute rate constants found through competitive studies differed substantially from those previously obtained during kinetic testing. Unusual behavior is observed for the comparison of results for substrate **8b**. In kinetic studies it was determined that **8b** was more reactive than **8a**, as reflected by the  $k_{\text{rel}}$  (Eq. 2) being greater than 1.0. However, in the competition study, **8b** was shown to be less reactive than **8a** with a  $k_{\text{rel}}$  of 0.62. One explanation for this observation is that the manganese(V)-oxo species is unlikely to serve as the sole active oxidant under catalytic conditions.

#### 4.2.4 Hammett Correlation Studies

The effect of the *para* substituents of each thioanisole have also been investigated for their effects on the manganese(IV)-corrole catalyzed sulfoxidation reactions to provide more insight into the mechanism. It was found that there is a significant dependence on the *para* substituent of substrates observed in Fig. 4-3. The Hammett correlation plot was based on the  $\log(k_{\text{rel}})$  from the competitive studies, versus the  $\sigma^+$  constants. Fig. 4-3 represents a linear correlation ( $R = 0.92$ ) for the oxidation reactions by  $\text{Mn}^{\text{IV}}(\text{TPC})\text{Cl}$  catalyst. Furthermore, the slope ( $\rho^+ = -1.75$ ) indicates a transition state involving charge separation in the rate-determining step because of its negative value. Together, discrepancies in the

data difference of kinetic and competitive studies, along with that of the Hammett correlation study, concludes that the manganese(V)-oxo species is not the sole active oxidant under catalytic conditions.

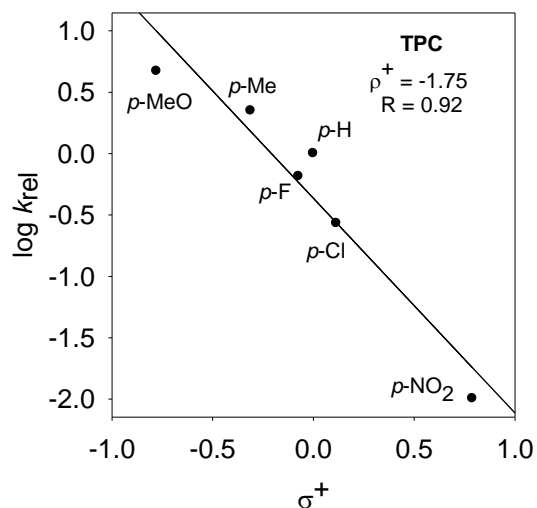


**Figure 4-3.** Hammett correlation studies ( $\log(k_{rel})$  vs  $\sigma^+$ ) for  $\text{Mn}^{\text{IV}}(\text{TPC})\text{Cl}$  (**3a**) catalyzed sulfoxidation of substituted thioanisoles by  $\text{PhI}(\text{OAc})_2$  in  $\text{CH}_3\text{OH}$  at  $23 \pm 2$  °C.

# CHAPTER 5

## CONCLUSION

In summary, a variety of manganese(III) corroles and manganese(IV) corroles were successfully synthesized and characterized spectroscopically. A new photochemical approach was developed to generate and study high-valent manganese-oxo model derivatives through visible light irradiation of the photo-labile bromate and chlorate precursors. This photochemistry is attributed to the homolytic cleavage of the respective O-Br bond of the bromate ligand or O-Cl bond of the chlorate ligand. As a result, one-electron oxidation of the manganese(IV) corroles generates the corresponding manganese(V)-oxo species as active oxygen atom transfer (OAT) agents. The phenomenal effect of the nature of the corrole ligand and solvent for the oxidation pathways was observed and discussed. Kinetic and spectral findings provided evidence to support the multiple oxidation pathways for the reactions of manganese(V)-oxo corroles with organic substrates.

Furthermore,  $[\text{Mn}^{\text{IV}}(\text{TPC})\text{Cl}]$  has been used as an efficient catalyst for the quantitative and selective oxidation of organic sulfides to sulfoxides with the mild oxidant  $\text{PhI}(\text{OAc})_2$  in the presence of a small amount of water. The corrole-manganese catalysts exhibit high reactivity, excellent chemoselectivity, and improved stability as attributed to the slow and steady-state formation of PhIO from  $\text{PhI}(\text{OAc})_2$ . Kinetic and Hammett correlation studies have both suggested that the elusive manganese(V)-oxo corrole intermediate is not the active oxidant under catalytic conditions.

Ultimately, the goals of this research were to develop greener methods for the mechanistic study of high-valent corrole-manganese-oxo intermediates and to improve methods for obtaining high-valent metal-oxo intermediates that can be used as highly efficient and selective catalyst for biomimetic oxidation reactions. Through photochemical studies, the use of visible-light for the generation of high-valent metal-oxo intermediates was found to be an environmentally conscience method due to not using terminal oxidants. Furthermore, catalytic studies, demonstrated the use of milder oxidants than previously reported in conjuncture with highly selective catalysts proved reliable in the efficient and selective biomimetic catalysis for the oxidation of organic sulfides. Resulting from these two studies, further investigations are underway in our laboratory to better define the mechanistic reaction pathways along with the application scope of manganese-corrole catalysts.

## REFERENCES

- (1) Axelrod, J.: The enzymatic demethylation of ephedrine. *J. Pharm.* **1955**, *114*, 430-438.
- (2) Guengerich, P. F.: Common and Uncommon Cytochrome P450 Reactions Related to Metabolism and Chemical Toxicity. *Chem. Res. Toxicol.* **2001**, *14*, 611-650.
- (3) *Cytochrome P450 Structure, Mechanism, and Biochemistry*: 3rd ed.; Ortiz de Montellano, P. R., Ed.; Kluwer Academic/Plenum: New York, 2005.
- (4) Poulos, T. L. F., B. C.; Howard, A. J.; : Crystal Structure of Substrate-Free *Pseudomonas Putida* Cytochrome P450. *J. Biochem.* **1986**, *25*, 5314-5322.
- (5) Guengerich, F. P.; Wu, Z.-L.; Bartleson, C. J.: Function of human cytochrome P450s: Characterization of the remaining orphans. *Biochem. Biophys. Res. Commun.* **2005**, *338*, 465-469.
- (6) Hasemann, C. A.; Kurumbail, R. G.; Boddupalli, S. S.; Peterson, J. A.; Deisenhofer, J.: Structure and Function of Cytochromes P450: A Comparative Analysis of Three Crystal Structures. *Structure* **1995**, *3*, 41-62.
- (7) Poulos, T. L. F., B. C.; Howard, A. J.: High-Resolution Crystal Structure of Cytochrome P450<sub>cam</sub>. *J. Mol. Biol.* **1987**, *195*, 687-700.
- (8) Marques, S.; Ramos, J. L.: Transcriptional Control of the *Pseudomonas putida* TOL plasmid catabolic pathways. *Mol. Microbiol.* **1993**, *9*, 923-929.
- (9) *Metal-Oxo and Metal-Peroxo Species in Catalytic Oxidations*; Meunier, B., Ed.; Springer-Verlag: Berlin, 2000.
- (10) Meunier, B.: Metalloporphyrins as Versatile Catalysts for Oxidation Reactions and Oxidative DNA Cleavage. *Chem. Rev.* **1992**, *92*, 1411-1456.

- (11) Sheldon, R. A.: *Metalloprophyrins In Catalytic Oxidations*; Marcel Dekker: New York, 1994.
- (12) Gross, Z.: High-valent corrole metal complexes. *J. Biol. Inorg. Chem.* **2001**, *6*, 733-738.
- (13) Liu, H.-Y.; Mahmood, M. H. R.; Qiuc, S.-X.; Chang, C. K.: Recent developments in manganese corrole chemistry. *Coord. Chem. Rev.* **2013**, *257*, 1306-1333.
- (14) Golubkov, G.; Bendix, J.; Gray, H. B.; Mahammed, A.; Goldberg, I.; DiBilio, A. J.; Gross, Z.: High-Valent Manganese Corroles and the First Perhalogenated Metalloporrole Catalyst. *Angew. Chem., Int. Ed.* **2001**, *40*, 2132-2134.
- (15) Bougher, C. J.; Liu, S.; Hicks, S. D.; Abu-Omar, M. M.: Valence Tautomerization of High-Valent Manganese(V)-Oxo Corrole Induced by Protonation of the Oxo Ligand. *J. Am. Chem. Soc.* **2015**, *137*, 14481–14487.
- (16) Wang, S. H.; Mandimutsira, B. S.; Todd, R.; Ramdhanie, B.; Fox, J. P.; Goldberg, D. P.: Catalytic Sulfoxidation and Epoxidation with a Mn(III) Triazacorrole: Evidence for A "Third Oxidant" in High-Valent Porphyrinoid Oxidations *J. Am. Chem. Soc.* **2004**, *126*, 18-19.
- (17) Johnson, A. W.; Kay, I. T.: 306. Corroles. Part I. Synthesis. *J. Chem. Soc* **1965**, 1620-1629.
- (18) Gross, Z.; Galili, N.; Simkhovich, L.; Saltsman, I.; Botoshansky, M.; Blaeser, D.; Boese, R.; Goldberg, I.: Solvent-Free Condensation of Pyrrole and Pentafluorobenzaldehyde: A Novel Synthetic Pathway to Corrole and Oligopyrromethenes. *Org. Lett.* **1999**, *1*, 599-602.

- (19) Gross, Z.; Simkhovich, L.; Galili, N.: First catalysis by corrole metal complexes: epoxidation, hydroxylation, and cyclopropanation. *Chem. Commun.* **1999**, 599-600.
- (20) Groves, J. T.: Reactivity and Mechanisms of Metalloporphyrin-Catalyzed Oxidations. *J. Porph. Phthal.* **2000**, *4*, 350-352.
- (21) Groves, J. T. K., William J., Jr.; Haushalter, Robert C.: Hydrocarbon oxidations with oxometalloporphyrins. Isolation and reactions of a (porphinato)manganese(V) complex. *J. Am. Chem. Soc.* **1980**, *102*, 6375-7.
- (22) Koszarna, B.; Gryko, D. T.: Efficient synthesis of meso-substituted corroles in a H<sub>2</sub>O-MeOH mixture. *J. Org. Chem.* **2006**, *71*, 3707-3717.
- (23) Maldotti, A.; Molinari, A.; Amadelli, R.: Photocatalysis with Organized Systems for the Oxofunctionalization of Hydrocarbons by O<sub>2</sub>. *Chem. Rev.* **2002**, *102*, 3811-3836.
- (24) Zhang, R.; Vanover, E.; Chen, T.-H.; Thompson, H.: Visible light-driven aerobic oxidation catalyzed by a diiron(IV)  $\mu$ -oxo biscorrole complex. *Appl. Catal. A* **2013**, *465*, 95-100.
- (25) Zhang, R.; Harischandra, D. N.; Newcomb, M.: Laser flash photolysis generation and kinetic studies of corrole-manganese(V)-oxo intermediates. *Chem. Eur. J.* **2005**, *11*, 5713-5720.
- (26) Zhang, R.; Newcomb, M.: Laser Flash Photolysis Formation and Direct Kinetic Studies of Manganese(V)-Oxo Porphyrin Intermediates. *J. Am. Chem. Soc.* **2003**, *125*, 12418-12419.

- (27) Zhang, R.; Horner, J. H.; Newcomb, M.: Laser Flash Photolysis Generation and Kinetic Studies of Porphyrin-Manganese-Oxo Intermediates. Rate Constants for Oxidations Effected by Porphyrin-Mn<sup>V</sup>-Oxo Species and Apparent Disproportionation Equilibrium Constants for Porphyrin-Mn<sup>IV</sup>-Oxo Species. *J. Am. Chem. Soc.* **2005**, *127*, 6573-6582.
- (28) Caron, S.; Dugger, R. W.; Ruggeri, S. G.; Ragan, J. A.; Ripin, D. H. B.: Large-Scale Oxidations in the Pharmaceutical Industry. *Chem. Rev.* **2006**, *106*, 2943-2989.
- (29) Baeckvall, J. E.: *Modern oxidation methods*; Wiley-VCH Verlag: Weinheim, 2004.
- (30) Hosseinpoor, F.; Golchubian, H.: Mn(III)-Catalyzed Oxidation of Sulfides to Sulfoxides with Hydrogen Peroxide. *Tetrahedron Lett.* **2006**, *47*, 5195-5197.
- (31) Kaczorowska, K.; Kolarska, Z.; Mitka, K.; Kowalski, P.: Oxidation of Sulfides to Sulfoxides. Part 2: Oxidation by Hydrogen Peroxide. *Tetrahedron Lett.* **2005**, *61*, 8315-8327.
- (32) Surendra, K.; Krishnaveni, N. S.; Kumar, V. P.; Sridhar, R.; Rao, K. R.: Selective and Efficient Oxidation of Sulfides to Sulfoxides with N-Bromosuccinimide in the Presence of Cyclodextrin in Water. *Tetrahedron Lett.* **2005**, *46*, 4581-4583.
- (33) Kumar, A.; Goldberg, I.; Botoshansky, M.; Buchman, Y.; Z., G.: Oxygen Atom Transfer Reactions from Isolated (Oxo)manganese(V) Corroles to Sulfides. *J. Am. Chem. Soc.* **2010**, *132*, 15233-15245.
- (34) Kwong, K. W.; Chen, T. H.; Luo, W.; Jeddi, H.; Zhang, R.: A biomimetic oxidation catalyzed by manganese(III) porphyrins and iodobenzene diacetate: Synthetic and mechanistic investigations. *Inorg. Chim. Acta* **2015**, *430*, 176-183.

- (35) Gross, Z.; Gray, H. B.: Oxidations catalyzed by metallocorroles. *Adv. Syn. Catal.* **2004**, *346*, 165-170.
- (36) Hodgkin, D. C.; Pickworth, J.; Robertson, J. H.; Trueblood, K. N.; Prosen, R. J.; White, J. G.: Structure of Vitamin B<sub>12</sub>: The Crystal Structure of the Hexacarboxylic Acid Derived from B<sub>12</sub> and the Molecular Structure of the Vitamin. *Nature* **1995**, *176*, 325-328.
- (37) Visser, S. P.; Ogliaro, F.; Gross, Z.; Shaik, S.: What is the Difference between the Manganese Porphyrin and Corrole Analogues of Cytochrome P450's Compound I? *Chem. Eur. J.* **2001**, *7*, 4954-4960.
- (38) Agadjanian, H.; Weaver, J. J.; Mahammed, A.; Rentsendorj, A.; Bass, S.; Kim, J.; Dmochowski, I. J.; Margalit, R.; Gray, H. B.; Gross, Z.; Medina-Kauwe, L. K.: Specific Delivery of Corroles to Cells via Noncovalent Conjugates with Viral Proteins. *Pharm. Res.* **2006**, *23*, 367-377.
- (39) Agadjanian, H.; Ma, J.; Rentsendorj, A.; Valluripalli, V.; Hwang, J. Y.; Mahammed, A.; Farkas, D. L.; Gray, H. B.; Gross, Z.; Medina-Kauwe, L. K.: Tumor Detection and Elimination by a Targeted Gallium Corrole. *Proc. Natl. Acad. Sci. U.S.A.* **2009**, *106*, 6105-6110.
- (40) Teo, R. D.; Gray, H. B.; Lim, P.; Termini, J.; Domeshek, E.; Gross, Z.: A Cytotoxic and Cytostatic Gold(III) Corrole. *Chem. Commun.* **2014**, *50*, 13789-13792.
- (41) Hwang, J. Y.; Lubow, J.; Chu, D.; Ma, J.; Agadjanian, H.; Sims, J.; Gray, H. B.; Gross, Z.; Farkas, D. L.; Medina-Kauwe, L. K.: Mechanistic Study of Tumor-Targeted Corrole Toxicity. *Mol. Pharm.* **2011**, *8*, 2233-2243.

- (42) Lim, P.; Mahammed, A.; Okun, Z.; Saltsman, I.; Gross, Z.; Gray, H. B.; Termini, J.: Differential Cytostatic and Cytotoxic Action of Metalloporphyrins against Human Cancer Cells: Potential Platforms for Anticancer Drug Development. *Chem. Res. Toxicol.* **2012**, *25*, 400-409.
- (43) Sims, J. D.; Hwang, J. Y.; Wagner, S.; Alonso-Valente, F.; Hanson, C.; Taguian, J. M.; Polo, R.; Harutyunyan, I.; Karapetyan, G.; Sorasaene, K.; Ibrahim, A.; Marban, E.; Moats, R.; Gray, H. B.; Gross, Z.; Medina-Kauwe, L. K.: A Porphyrin Nanobiologic Elicits Tissue-Activated MRI Contrast Enhancement and Tumor-Targeted Toxicity. *J. Control. Release* **2015**, *217*, 92-101.
- (44) Haber, A.; Gross, Z.: Catalytic Antioxidant Therapy by Metalloporphyrins: Lessons from Metalloporphyrins. *Chem. Commun.* **2015**, *51*, 5812-5827.
- (45) Okun, Z.; Gross, Z.: Fine Tuning the Reactivity of Porphyrin-Based Catalytic Antioxidants. *J. Inorg. Chem.* **2012**, *51*, 8083-8090.
- (46) Okun, Z.; Kupersmidt, L.; Amit, T.; Mandel, S.; Bar-Am, O.; Youdim, M. B. H.; Gross, Z.: Manganese Porphyrins Prevent Intracellular Nitration and Subsequent Death of Insulin-Producing Cells. *ACS Chem. Biol.* **2009**, *4*, 910-914.
- (47) Gross, Z.; Golubkov, G.; Simkhovich, L.: Epoxidation catalysis by a manganese porphyrin and isolation of an oxomanganese(V) porphyrin. *Angew. Chem. Int. Ed. Engl.* **2000**, *39*, 4045-4047.
- (48) Suslick, K. S.; Watson, R. A.: The photochemistry of chromium, manganese, and iron porphyrin complexes. *New J. Chem.* **1992**, *16*, 633-42.

- (49) Zhang, R.; Newcomb, M.: Laser Flash Photolysis Generation of High-Valent Transition Metal-Oxo Species: Insights from Kinetic Studies in Real Time. *Acc. Chem. Res.* **2008**, *41*, 468-477.
- (50) Pan, Z.; Wang, Q.; Sheng, X.; Horner, J. H.; Newcomb, M.: Highly Reactive Porphyrin–Iron–Oxo Derivatives Produced by Photolyses of Metastable Porphyrin–Iron(IV) Dipchlorates. *J. Am. Chem. Soc.* **2009**, *131*, 2621-2628.
- (51) Che, C.-M.; Huang, J.-S.: Metalloporphyrin-based oxidation systems: from bioimetic reactions to application in organic synthesis. *Chem. Commun.* **2009**, 3996-4015.
- (52) Liu, H. Y.; Lai, T. S.; Yeung, L. L.; Chang, C. K.: First Synthesis of Perfluorinated Corrole and its Mn=O Complex. *Org. Lett.* **2003**, *5*, 617-620.
- (53) Hansch, C.; Leo, A.; Taft, R. W.: A survey of Hammett substituent constants and resonance and field parameters. *Chem. Rev.* **1991**, *91*, 165-195.
- (54) Carreno, C. M.: Applications of Sulfoxides to Asymmetric Synthesis of Biologically Active Compounds. *Chem. Rev.* **1995**, *95*, 1717-1760.
- (55) Baeckvall, J. E.: Modern Oxidation Methods. **2010**.
- (56) Eikey, R. A.; Khan, S. I.; Abu-Omar, M. M.: The elusive terminal imido of manganese(v). *Angew. Chem., Int. Ed.* **2002**, *41*, 3592-3295.
- (57) Edwards, N. Y.; Eikey, R. A.; Loring, M. I.; Abu-Omar, M. M.: High-valent imido complexes of manganese and chromium corroles. *Inorg. Chem.* **2005**, *44*, 3700-3708.
- (58) Golubkov, G.; Gross, Z.: Nitrogen Atom Transfer between Manganese Complexes of Salen, Porphyrin, and Corrole and Characterization of a (Nitrido)manganese(VI) Corrole. *J. Am. Chem. Soc.* **2005**, *127*, 3258–3259.

(59) Yu, L.; Wang, Q.; Dai, L.; Li, W.-Y.; Chen, R.; Mahmood, M. H. R.; Liu, H.-Y.; Chang, C.-K.: Solvent Effects On Oxygen Atom Transfer Reaction Between Manganese(V)-oxo Corrole and Alkene. *Chem. Lett* **2013**, *24*, 447-449.

(60) Zhang, R.; Huang, Y.; Abebrese, C.; Thompson, H.; Vanover, E.; Webb, C.: Generation of trans-dioxoruthenium(VI) porphyrins: A photochemical approach. *Inorg. Chim. Acta* **2011**, *372*, 152-157.

(61) Kwong, K.; Lee, N. F.; Ranburger, D.; Malone, J.; Zhang, R.: Visible Light-Induced Formation of Corrole-Manganese(V)-oxo Complexes: Observation of Multiple Oxidation Pathways. *J. Inorg. Biochem.* **2016**, *163*, 39-44.

# CURRICULUM VITAE

## EDUCATION

---

- MS in Chemistry: Western Kentucky University, USA, 2017-2018
- BS in Chemistry and Biology: Western Kentucky University, USA, 2013-2017

## RESEARCH EXPERIENCE

---

- Graduate Research Assistant, Western Kentucky University, USA, 2017-Present
  - Project: *Visible Light Generation of High-Valent Corrole-Manganese(V)-Oxo Intermediates and Biomimetic Studies of the Oxidation of Organic Sulfides Catalyzed by Manganese Corroles with Iodobenzene Diacetate*
- Graduate Teaching Assistant, Western Kentucky University, USA, 2017-Present
  - Organic Chemistry I and II
- Undergraduate Research Assistant, Western Kentucky University, USA, 2015-2017
- Undergraduate Teaching Assistant, Western Kentucky University, USA, 2017

## PEER-REVIEWED JOURNAL PUBLICATIONS

---

- Chen, T.-H.; Kwong, K. W.; Ranburger, D.; Zhang, R., Highly efficient and chemoselective oxidation of sulfides catalyzed by iron(III) corroles with iodobenzene diacetate. *Inorg. Chim. Acta.* **2016**, *451*, 65-72
- Kwong, K. W.; Lee, N. F.; Ranburger, D.; Malone, J.; Zhang, R., Visible light-induced formation of corrole-manganese(V)-oxo complexes: Observation of multiple oxidation pathways. *J. Inorg. Biochem.* **2016**, *163*, 39-44

## **PEER-REVIEWED JOURNAL PUBLICATIONS**

---

- **Oral Presentation: 2018 WKU Student Research Conference** **2018**
  - Photochemical and Catalytic Study of Manganese Corrole Complexes as Biomimetic Catalysts
- **Oral Presentation: Southeastern Regional Meeting of the American Chemical Society** **2017**
  - Photochemical Generation of High-Valent Metal-Oxo Corroles by Visible Light Irradiation of Manganese(IV) Corrole Bromate Species
- **Poster Presentation: 2016 WKU Student Research Conference** **2016**
  - Synthetic and Spectral Studies of Manganese 5,10,15-*tris*(pentafluorophenyl)corrole

## **EXTRACURRICULAR ACTIVITIES**

---

- **Marathon Running** **10/16-Present**
  - Bowling Green 26.2, Bowling Green, KY (26.2 miles)
  - Mountain Mist 50 K, Huntsville, AL (50 kilometers)
  - Stump Jump 50 K, Chattanooga, TN (52 kilometers)
  - New York City Marathon, New York City, NY (26.2 miles).
- **WKU Men's Swimming Team** **8/13-4/15**

## LIST OF ABBREVIATIONS

---

$[(4\text{-BrC}_5\text{H}_4)_3\text{N}]\text{SbCl}_6$	<i>tris</i> -(4-bromophenyl)ammoniumyl hexachloroantimonate
Ac <sub>2</sub> O	Acetic anhydride
Ar	Aryl
Ag(BrO <sub>3</sub> )	Silver bromate
Ag(ClO <sub>3</sub> )	Silver chlorate
Al <sub>2</sub> O <sub>3</sub>	Aluminum oxide
BF <sub>3</sub> ·OEt <sub>2</sub>	Boron trifluoride diethyl etherate
cam	Camphor
CDCl <sub>3</sub>	Deuterated chloroform
CH <sub>2</sub> Cl <sub>2</sub>	Dichloromethane
CHCl <sub>3</sub>	Chloroform
CH <sub>3</sub> CN	Acetonitrile
CH <sub>3</sub> OH	Methanol
CYP450s	Cytochrome P450 enzymes
DDQ	2,3-Dichloro-5,6-dicyano- <i>p</i> -benzequinone
DMF	<i>N,N</i> -Dimethylformamide
ESI-MS	Electrospray ionization-mass spectroscopy
Fe <sup>III</sup> (Cor)	Iron(III) corrole complexes
Fe <sup>IV</sup> (TPFC)	Iron(IV) 5,10,15- <i>tris</i> (pentafluorophenyl)corrole
GC-MS	Gas chromatography-mass spectrometry

$^1\text{H-NMR}$	Proton nuclear magnetic resonance
HOAc	Acetic acid
$\text{H}_3\text{TPC}$	5,10,15-triphenylcorrole
$\text{H}_3\text{TPFC}$	5,10,15- <i>tris</i> (pentafluorophenyl)corrole
$\text{H}_3(4\text{-NO}_2)\text{TPC}$	5,10,15- <i>tris</i> (4-nitrophenyl)corrole
$k_0$	Background rate constant
$k_{\text{ox}}$	Second-order rate constant
$k_{\text{obs}}$	Observed pseudo-first-order rate constant
$k_{\text{rel}}$	Relative rate constant
$[\text{M}]^+$	Molecular ion
$[\text{M} - \text{Cl}]^+$	Molecular ion minus chlorine ligand
<i>m</i> CPBA	<i>meta</i> -Chloroperbenzoic acid
$\text{Mn}^{\text{III}}(\text{TPC})$	Manganese(III) 5,10,15-triphenylcorrole chloride
$\text{Mn}^{\text{III}}(\text{TPFC})$	Manganese(III) 5,10,15- <i>tris</i> (pentafluorophenyl)corrole chloride
$\text{Mn}^{\text{III}}(4\text{-NO}_2\text{TPC})$	Manganese(III) 5,10,15- <i>tris</i> (4-nitrophenyl)corrole chloride
$\text{Mn}^{\text{IV}}(\text{Cor})\text{Cl}$	Manganese(IV) corrole complexes
$\text{Mn}^{\text{IV}}(\text{Cor})\text{BrO}_3$	Manganese(IV) corrole bromate
$\text{Mn}^{\text{IV}}(\text{Cor})\text{ClO}_3$	Manganese(IV) corrole chlorate
$\text{Mn}^{\text{IV}}(\text{TPC})\text{Cl}$	Manganese(IV) 5,10,15-triphenylcorrole chloride
$\text{Mn}^{\text{IV}}(\text{TPFC})\text{Cl}$	Manganese(IV) 5,10,15- <i>tris</i> (pentafluorophenyl)corrole chloride

Mn <sup>IV</sup> (4-NO <sub>2</sub> TPC)Cl	Manganese(IV) 5,10,15- <i>tris</i> (4-nitrophenyl)corrole chloride
Mn <sup>V</sup> (Cor)O	Corrole-manganese(V)-oxo
Mn <sup>VI</sup> (Cor)O	Corrole-manganese(VI)-oxo
<i>m/z</i>	Mass-charge ratio
Na <sub>2</sub> SO <sub>4</sub>	Sodium sulfate
NADH	Nicotinamide adenine dinucleotide
NADPH	Nicotinamide adenine dinucleotide phosphate
OAT	Oxygen atom transfer
PhIO	Iodosylbenzene
PhI(OAc) <sub>2</sub>	Iodobenzene diacetate
ppm	Parts per million
$\rho^+$	Slope of Hammett correlation plot
$\sigma^+$	Hammett substituent constant
Sub	Substrate
TLC	Thin layer chromatography
TMS	Tetramethylsilane
TPC	5,10,15- <i>tris</i> phenylcorrole system
TPFC	5,10,15- <i>tris</i> (pentafluorophenyl)corrole system
UV-vis	Ultraviolet-visible
W	Watts

---